STEAM INJECTION INTO WATER-SATURATED POROUS ROCK

J. BRUINING, D. MARCHESIN, AND C.J. VAN DUIJN

Abstract. We formulate conservation laws governing steam injection in a linear porous medium containing water. Heat losses to the outside are neglected. We study the condensation front as a travelling wave, under the approximation that pressure variations are negligible within this front. We find this travelling wave for the case of injection of high quality steam using a combination of linearized analysis at equilibria and numerical calculation of orbits.

We find a complete and systematic description of all solutions of the Riemann problem for the injection of a mixture of steam and water into a water-saturated porous medium. For ambient pressure, there are three kinds of solutions, depending on injection and reservoir conditions. We show that the solution is unique for each initial data.

Introduction

Steam injection is an effective technique to restore groundwater aquifers contaminated with non-aqueous phase liquids (NAPLs) such as hydrocarbon fuels and halogenated hydrocarbons [25]. It is also one of the most effective methods to recover oil from medium to heavy oil reservoirs [22]. The main feature of steam injection is the steam condensation front (SCF), which marks the boundary between the upstream zone at boiling temperature and the downstream liquid zone below the boiling temperature. Depending on the situation there may exist an isothermal steam-water shock at the boiling temperature ($HISW$) instead of the SCF. The main result of this work is a complete and systematic classification of the structure of all possible cases of Riemann solutions.

There is an extensive literature on models of steam drive. The weak point of all these models is the need to introduce insufficiently justified extraneous assumptions to close the model. Marx and Langenheim [16] use the energy balance including heat losses to cap and base rock to derive expressions for the velocity of the condensation front. In their classic paper, Mandl and Volek [15], extend the work of Marx and Langenheim with a thorough analysis of the behavior of the condensation front. They find that after a critical time the heat flow out of the condensation front, which was conductive before the critical time, becomes convective leading to the formation of a hot water tongue. Lacking experimental information, they use integrated mass balance equations, closed by the assumption that all water condensed due to heat losses flows along with the steam to the condensation front. Shutler [26] proposed a relatively simple model which treats the oil saturation in the steam zone as an unknown. In this model again a condensation front is present separating an upstream steam zone from a downstream oil–water zone. It is assumed that all steam condenses at the SCF. The velocity of the SCF follows from a local heat balance. Water

Key words and phrases. Porous medium, steamflood, travelling waves, multiphase flow.

This work was supported in part by: CNPq under Grant 300204/83-3, FINEP under CTPETRO Grant 21.01.0248.00; NWO under Fellowship Grant R 75-389, The Netherlands; IMA (Univ. of Minnesota), Dietz Laboratory (TU Delft, The Netherlands), IMPA (Brazil).

and oil conservation equations applied at the SCF are insufficient to close the problem and reference [26] uses the remediation of assuming a constant connate water saturation in the steam zone.

Bruining and Van Duijn [6] show through a detailed mathematical analysis that a model of the steam condensation process is required to close the problem. However, they assume thermodynamic equilibrium between the vapor and water leading to a "delta function" distribution condensation in the short condensation zone. Also, reference [6] decouples the mass and heat balance equations by the assumption of saturation independent heat capacities. Yortsos [33] combines heat balance with heat losses and mass balance equations to derive semi-analytical expressions for the saturation distribution. A constant steam temperature upstream of the condensation front and a temperature decrease from the boiling temperature to the original reservoir temperature in the liquid zone describes the flow. Other models related to the one of Shutler have been proposed e.g. by Aydelotte and Pope [1] and Wingard and Orr [32]. The formulations of the steam drive models are by no means complete. Since the seventies there is a large literature on numerical methods for problems containing regions where the variables change rapidly. A recent engineering paper concerning this problem applied to steam is in [28]. Standard numerical simulators, however, fail to provide details of the steam behavior in the presence of multi-component mixtures in the SCF even if enough resolution were used.

Little interest has been given to the precise mechanisms that occur in the condensation zone with the papers of Stewart and Udell (1988), Menegus and Udell (1985) and Udell (1985) as notable exceptions. This work is an interesting step in the right direction albeit that use a traveling wave approach without connecting the solution to the upstream and downstream rarefaction part of the solution.

Saturation distributions are affected by the precise interplay of heat and mass transfer with capillary forces [6]. The latter mechanisms, which are diffusive and operate mainly in a very short region, affect also the global solution. This fact has been recognized in the mathematical literature at least since [13]. Consequently, numerical solutions that do not respect the detailed behavior in the steam zone can give erroneous results as they reflect numerical rather than physical diffusions.

This paper combines the global behavior of the steam condensation process with the local behavior of the steam condensation zone. This is again accomplished the method of *matched asymptotic expansions* [10], with the inner solution describing the steam condensation process and the outer solution describing the non-condensing steam flow upstream and the cold fluid flow downstream.

Here, the spatial and time scales of a non-equilibrium kinetic model are resolved within the inner solution. Thus, the assumption of thermodynamic equilibrium within the inner solution is avoided. We propose a linear condensation rate equation based on concepts explained in reference [20]. However, our framework would be able to accommodate more realistic condensation rate equations. Of course, a condition of the rate equation is that thermodynamic equilibrium is attained in the limit of infinite mass transfer rates.

In this article we limit ourselves to the simple case of steam displacing water. Our aim is to investigate whether such a condensation rate model leads to a unique well posed solution of the Riemann problem for all possible values of the model parameters, providing mathematical validation of our model.

In Section 1, the physical model is presented. It is described mathematically by balance equations of mass and thermal energy, which are rewritten into a form suitable for analysis.

Section 2 presents the basic waves arising in the model; the main concern is to identify their speeds, so as to be able to find the order in which they may appear in a linear steam injection experiment. In Section 3, we see that for certain values of initial and boundary data, some of these speeds coincide, giving rise to bifurcation and structural change in the Riemann solution. All solutions of the Riemann problem are in Section 4.

Section 5 verifies that the SCF satisfies Lax's shock inequalities, but not strictly.

Section 6 summarizes our results and conclusions.

The appendices A to F contain detailed analysis and numerical calculations for understanding the internal structure of the SCF as a travelling wave.

In Appendix A the ODE's for the travelling wave are presented. In Appendix B the neighborhood of the phase portrait near the equilibria are analyzed. The analysis for the case of injection of pure steam is treated in Appendix C. The analysis for simultaneous water and steam injection is treated in Appendix D. In Appendix E a travelling wave model of the steam condensation front is made. In Appendix F the phase portrait is presented for the injection of pure steam.

Appendix G describes notation and values for the physical quantities appearing in the model.

1. Physical and mathematical model

1.1. **Physical model.** We consider linear steam displacement in a homogeneous reservoir of constant permeability and porosity. The reservoir is initially saturated with water. The pressure gradients $\partial p_w/\partial x$, $\partial p_g/\partial x$ driving the fluids are small with respect to the prevailing system pressure p divided by the length of the reservoir. In particular, within the short steam condensation zone pressure variations are negligible. Hence we disregard the effect of pressure variation on the density of the fluids and on their thermodynamic properties. The reservoir is horizontal, so gravitational effects vanish.

A steam-water mixture is injected at constant rate u^{inj} and constant composition. Transverse heat losses are disregarded. We neglect capillary forces after steam breakthrough at the production end of the reservoir to avoid problems with the capillary end effect, which is outside the present scope of our interest.

The effects of temperature on the fluid properties, *e.g.* water viscosity μ_w and steam viscosity μ_g, are taken into account. The temperature dependence of the liquid water density ρ_w and of the steam density ρ_g is taken into account. Darcy's Law determines the fluid motion. We include capillary pressure effects. The temperature dependence of heat capacities and of the evaporation heat are taken into account. Also, an effective longitudinal heat *conduction* term is taken into account.

We have chosen to describe condensation in terms of a steam mass condensation rate equation. The mass condensation rate q is always positive when the temperature drops below the boiling temperature T^b as long as not all steam has condensed, that is $S_w < 1$.

The stated conditions can be considered representative of steam injection in the subsurface for remediation of contaminated sites. As steam is injected the reservoir is heated. Depending on the proportions of steam and water in the injected mixture, we can distinguish three regimes, which differ in the structure of Riemann solutions. When steam of 100% quality is injected, there will be a decrease of the steam saturation in the hot zone away from the

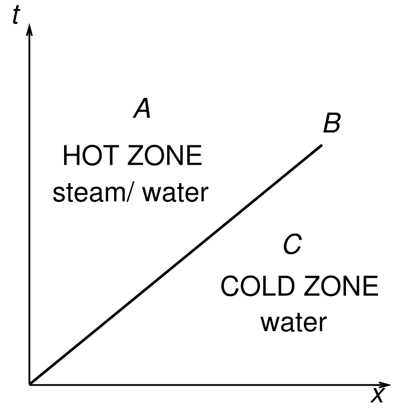

FIGURE 1.1. B: Condensation front or cooling front

injection point (described mathematically as a rarefaction wave) and then a SCF to the cold water (described mathematically as a shock with a concentrated source term). This is called situation *I*. As the water injection rate is increased further a zone in which the steam saturation is constant will develop preceding the rarefaction until the steam saturation in the hot zone is constant. After this constant state there is a SCF and a cold water region. This will be called situation *II*. Finally when the water–steam injection ratio is increased further, the steam bank will not be fast enough to reach the cooling front separating the hot and cold water zones; thus there is no SCF. This and higher ratios originate in situation *III*. In all regimes, there is a hot zone and a cool zone, whose boundary moves with constant speed, as shown in Fig. 1.1.

Each of the enthalpies per unit volume $H_w(T)$, $H_r(T)$, $H_g(T)$ ($[J/kg]$) is defined with respect to the enthalpy at the initial reservoir temperature T^0 at the standard state. This means that they are all zero at the initial temperature T^0. The enthalpy of steam is subdivided in a sensible part $H_g^s(T)$ and a latent part $H_g^l(T^0)$, *i.e.* $H_g(T) = H_g^s(T) + H_g^l(T^0)$. The sensible heat $H_g^s(T^0)$ is zero at the initial reservoir temperature. The evaporation heat or the latent heat per unit mass at the initial reservoir temperature T^0 is denoted by

$$\Lambda^0 = \Lambda(T^0) = H_g^l(T^0)/\rho_g(T^0). \tag{1.1}$$

In general $\Lambda(T)$ is the evaporation heat per unit mass at temperature T. The enthalpies as a function of temperature are obtained from correlations given in reference [29] and summarized in Appendix G for convenience.

We assume Darcy's law for multiphase flow, without gravity terms:

$$u_w = -\frac{kk_{rw}}{\mu_w}\frac{\partial p_w}{\partial x}, \qquad u_g = -\frac{kk_{rg}}{\mu_g}\frac{\partial p_g}{\partial x}. \tag{1.2}$$

We use an average value for the absolute permeability for sand (see Appendix G). The relative permeability functions k_{rw} and k_{rg} are considered to be power functions of their respective effective saturations [9], *i.e.* $S_{we} = (S_w - S_{wc})/(1 - S_{wc})$, $S_{ge} = S_g/(1 - S_{wc})$ (see Appendix G). The effective saturations require knowing the connate water saturation S_{wc}. In all our examples we use a fourth power of the effective saturation for the relative water permeability and a quadratic dependence for the steam relative permeability. We use a porosity φ that is representative for unconsolidated sand.

The composite thermal conductivity depends on the rock, water and steam heat conductivities κ_r, κ_w and κ_g, (see Appendix G).

The liquid water viscosity and the steam viscosity are temperature-dependent functions (see Appendix G). We also use the Brooks-Corey power law dependence of the capillary pressure on saturation (see Appendix G).

The water mass source term is taken as

$$q = \begin{cases} q_b(T - T^b)(S_w - 1) & \text{for} \quad T \leq T^b, \quad 0 \leq S_w \leq 1; \\ 0 & \text{otherwise.} \end{cases} \tag{1.3}$$

This term is motivated by the idea that the condensation rate is determined by a "driving force" which is proportional to its departure from equilibrium $S_w = 1$ and $T = T^b$ (see also reference [20]).

The value of q_b is considered very large as diffusion processes within a pore may occur at characteristic time $t_{char} \approx (\Delta x)^2/D = 10^{-8}/10^{-5} = 1$ millisecond, where $\Delta x = 10^{-4}$ m is a typical pore diameter and the diffusion coefficient D in water vapor is approximately 10^{-5} [m^2/s] (see [4]).

1.2. **The model equations.** The mass balance equation of liquid water and steam read as follows:

$$\frac{\partial(\varphi \rho_w S_w)}{\partial t} + \frac{\partial(\rho_w u_w)}{\partial x} = q, \tag{1.4}$$

$$\frac{\partial(\varphi \rho_g S_g)}{\partial t} + \frac{\partial(\rho_g u_g)}{\partial x} = -q. \tag{1.5}$$

The rock porosity φ is assumed to be constant. We include longitudinal heat conduction, but neglect heat losses to the surrounding rock, in the energy balance equation given below. By our assumption of almost constant pressure we ignore adiabatic compression and decompression effects. Thus the energy balance is (See reference [4], Table 10.4-1):

$$\frac{\partial}{\partial t}(H_r + \varphi S_w H_w + \varphi S_g H_g) + \frac{\partial}{\partial x}(u_w H_w + u_g H_g) = \frac{\partial}{\partial x}\left(\kappa \frac{\partial T}{\partial x}\right). \tag{1.6}$$

Here κ is the composite conductivity of the rock–fluid system [2]:

$$\kappa = \kappa_r + \varphi(S_w \kappa_w + S_g \kappa_g). \tag{1.7}$$

Equations (1.4), (1.5), and (1.6) are the basic governing equations for the flow.

Equations (1.4) and (1.5) are combined with the heat balance equation (1.6), where we also use separation in sensible and latent quantities, to obtain:

$$\begin{aligned} &\frac{\partial}{\partial t}\left(H_r + \varphi S_w H_w + \varphi S_g H_g^s\right) + \frac{\partial}{\partial x}\left(u_w H_w + u_g H_g^s\right) - \frac{\partial}{\partial x}\left(\kappa \frac{\partial T}{\partial x}\right) = \\ &= -\frac{\partial}{\partial t}\left(\varphi S_g H_g^l\right) - \frac{\partial}{\partial x}\left(u_g H_g^l\right) = -\frac{\partial}{\partial t}\left(\varphi S_g \rho_g \Lambda^0\right) - \frac{\partial}{\partial x}\left(u_g \rho_g \Lambda^0\right) = \\ &= -\Lambda^0\left(\frac{\partial}{\partial t}\left(\varphi S_g \rho_g\right) + \frac{\partial}{\partial x}\left(u_g \rho_g\right)\right). \end{aligned}$$

Using Eq. (1.5), this yields

$$\frac{\partial}{\partial t}\left(H_r + \varphi S_w H_w + \varphi S_g H_g^s\right) + \frac{\partial}{\partial x}\left(u_w H_w + u_g H_g^s\right) = q\Lambda^0 + \frac{\partial}{\partial x}\left(\kappa \frac{\partial T}{\partial x}\right). \tag{1.8}$$

The capillary pressure

$$P_c = P_c(S_w) = p_g - p_w \tag{1.9}$$

which is given by Equation (G.12), is a strictly monotone decreasing function; it appears in the definition of the capillary diffusion coefficient Ω:

$$\Omega = -f_w \frac{k k_{rg}}{\mu_g} \frac{dP_c}{dS_w} \geq 0. \tag{1.10}$$

We notice that Ω vanishes precisely at water saturations $S_w = S_{wc}$ and $S_w = 1$.

Let us define the fractional flow functions for water and steam:

$$f_w = \frac{k_{rw}/\mu_w}{k_{rw}/\mu_w + k_{rg}/\mu_g}, \qquad f_g = \frac{k_{rg}/\mu_g}{k_{rw}/\mu_w + k_{rg}/\mu_g}. \tag{1.11}$$

Using Darcy's law (1.2) (in the absence of gravitational effects) and the definition of P_c given in Eq. (1.9), one can easily show from Eqs. (1.2) and (1.10) that:

$$u_w = u f_w - \Omega \frac{\partial S_w}{\partial x}, \qquad u_g = u f_g - \Omega \frac{\partial S_g}{\partial x}, \tag{1.12}$$

where

$$u = u_w + u_g \tag{1.13}$$

is the *total* or *Darcy velocity* and Ω acts as a saturation-dependent capillary diffusion coefficient.

Substituting (1.12) into Equations (1.4), (1.5) and (1.8) leads to

$$\varphi \frac{\partial\left(\rho_w S_w\right)}{\partial t} + \frac{\partial\left(\rho_w u f_w\right)}{\partial x} = q + \frac{\partial}{\partial x}\left(\rho_w \Omega \frac{\partial S_w}{\partial x}\right), \tag{1.14}$$

$$\varphi \frac{\partial\left(\rho_g S_g\right)}{\partial t} + \frac{\partial\left(\rho_g u f_g\right)}{\partial x} = -q + \frac{\partial}{\partial x}\left(\rho_g \Omega \frac{\partial S_g}{\partial x}\right), \tag{1.15}$$

$$\begin{aligned}\frac{\partial}{\partial t}\left(H_r + \varphi H_w S_w + \varphi H_g^s S_g\right) + \frac{\partial}{\partial x}\Big(u\left(H_w f_w + H_g^s f_g\right)\Big) = \\ = q\Lambda^0 + \frac{\partial}{\partial x}\left(\left(H_w - H_g^s\right)\Omega \frac{\partial S_w}{\partial x}\right) + \frac{\partial}{\partial x}\left(\kappa \frac{\partial T}{\partial x}\right).\end{aligned} \tag{1.16}$$

The governing system of equations is (1.14)–(1.16).

As to initial conditions, we assume that the reservoir is filled with water at saturation $S_w(x, t=0) = S_w^0 = 1$ with constant temperature $T(x, t=0) = T^0$. As to boundary conditions, the total injection rate u^{inj} is specified and constant (see Appendix G). The steam-water injection ratio is specified in terms of the water saturation S_w^{inj} at the injection side.

Remark 1. *Consider a situation for which the temperature is constant. Then the enthalpies are constant, so Eq. (1.8) becomes*

$$\varphi H_w \frac{\partial S_w}{\partial t} + \varphi H_g^s \frac{\partial S_g}{\partial t} + H_w \frac{\partial u_w}{\partial x} + H_g^s \frac{\partial u_g}{\partial x} = q\Lambda^0. \tag{1.17}$$

We regroup Eq. (1.17) and use the mass balance equations (1.4) and (1.5). Since the temperature is constant the densities are constant too, so Eq. (1.17) becomes

$$\begin{aligned} H_w\left(\varphi\frac{\partial S_w}{\partial t} + \frac{\partial u_w}{\partial x}\right) + H_g^s\left(\varphi\frac{\partial S_g}{\partial t} + \frac{\partial u_w}{\partial x}\right) &= q\Lambda^0, \\ \frac{H_w}{\rho_w}q - \frac{H_g^s}{\rho_{w,g}}q &= q\Lambda^0, \\ \left(\frac{H_w}{\rho_w} - \frac{H_g^s}{\rho_{w,g}} - \Lambda^0\right) q &= 0. \end{aligned} \tag{1.18}$$

The term in parenthesis in Eq. (1.18) is minus the enthalpy per unit mass required to convert water into steam and is therefore non-zero. Consequently we must have that $q = 0$. Summarizing, we can say that if the temperature is constant in space and time then there is no source term.

2. The hyperbolic framework

By ignoring capillary pressure and heat conduction diffusive effects, we are in the framework of first order hyperbolic conservation laws; this framework is useful to study the basic waves of the model. Throughout this section we assume that all fluids are in thermodynamic equilibrium. Equations (1.14) and (1.15), the mass balance equation of liquid water and steam combined with Darcy's law read as follows:

$$\frac{\partial(\varphi\rho_w S_w)}{\partial t} + \frac{\partial(\rho_w u f_w)}{\partial x} = q, \tag{2.1}$$

$$\frac{\partial(\varphi\rho_g S_g)}{\partial t} + \frac{\partial(\rho_g u f_g)}{\partial x} = -q. \tag{2.2}$$

When we add these equations, we obtain the total water conservation:

$$\varphi\frac{\partial}{\partial t}(\rho_w S_w + \rho_g S_g) + \frac{\partial}{\partial x}\Big(u(\rho_w f_w + \rho_g f_g)\Big) = 0. \tag{2.3}$$

Eq. (1.16) becomes

$$\frac{\partial}{\partial t}\left(H_r + \varphi H_w S_w + \varphi H_g^s S_g\right) + \frac{\partial}{\partial x}\Big(u(H_w f_w + H_g^s f_g)\Big) = q\Lambda^0, \tag{2.4}$$

or equivalently, as in Eq. (1.6)

$$\frac{\partial}{\partial t}(H_r + \varphi H_w S_w + \varphi H_g S_g) + \frac{\partial}{\partial x}\Big(u(H_w f_w + H_g f_g)\Big) = 0. \tag{2.5}$$

Eqs. (2.3) and (2.4) will be used for most of the analysis in this section.

Remark 2. *Notice that all speeds defined by Equations (2.3) and (2.4) are proportional to u. Thus we can choose any speed to parameterize all the other ones.*

Let us consider all regions where the mass transfer term vanishes. The mass transfer can vanish because of several reasons. Based on this reasons, we classify the regions in the following table. Because the mass source term vanishes (Eq. (1.3)), we have the following zones in the reservoir:

$S_w \backslash T$	$T = T^b$	$T < T^b$
$S_w < 1$	hot steam zone	xxxxxxxxxxxxxx
$S_w = 1$	hot water zone	cold water zone

Table 1: Classification according to mass source term.

Definition 2.1. We call "hot steam-water region", or "hot region", the hot steam zone together with hot water zone, where $T = T^b$. We call "liquid water region" the hot water zone together with the cold water zone.

These regions overlap on the hot water zone.

Remark 3. *There is no "cold steam zone" in Table 1 because at thermodynamical equilibrium steam cannot exist at a temperature lower than T^b.*

As we will see, a configuration composed by sequential zones of hot steam, hot water and cold water is possible, counting away from the injection point. At the first interface $S_w = 1$ is reached, while at the second one $T = T^0$ is reached.

A configuration containing only the hot steam zone and the cold water zone is possible if we interpose the so called SCF, where both saturation and temperature change abruptly.

Remark 4. *The source term in the hot region and in the liquid water region is zero. That the source term is zero in the hot region follows from Remark 1. That the source term is zero in the liquid region follows from the existence of a single phase and consequent absence of mass and energy transfer between phases.*

2.1. **The hot region.** This region starts with the hot steam zone, where steam is injected at boiling temperature T^b. We claim that the Darcy velocity u (given by Eq. (1.13)) in the hot region is independent of position. To prove this fact we use equations (2.1), (2.2). As the temperature is T^b, the source term (such as given in Eq. (1.3)) vanishes and the densities are constant. We can divide Eqs. (2.1), (2.2) by the densities and add the resulting equations and obtain our claim.

Since the Darcy velocity u is a constant in space in the hot region and since in this work we also take that u^{inj} is constant in time, the temperature T^b and the Darcy velocity u^b are constant in this region. Thus Eq. (2.4) is satisfied trivially, and both Eqs. (2.1) and (2.2) reduce to the same Buckley-Leverett problem for steam and water that follows:

$$\varphi \frac{\partial S_w}{\partial t} + u^b \frac{\partial f_w}{\partial x} = 0. \tag{2.6}$$

This equation governs propagation in the hot steam zone, as long as steam and water are both present. The classical Oleĭnik construction [18], or equivalently, the fractional flow theory [21] describe waves in this zone.

We will denote by v_s^b the speed of propagation of saturation waves in the hot steam zone. It is obtained from Eq. (2.6) as the characteristic speed:

$$v_s^b = v_s^b(S_w; u^b) = \frac{u^b}{\varphi}\frac{\partial f_w^b}{\partial S_w}(S_w), \tag{2.7}$$

where $T = T^b$ and we use the nomenclature $f_w^b(S_w) = f_w(S_w, T_b)$.

A particular Buckley-Leverett shock for (2.6) turns out to play a relevant role, separating a mixture of steam and water from pure water, both at boiling temperature. We call it the *hot isothermal steam-water shock* or *HISW* shock between the $(-)$ state (S_w^b, T^b, u^b) containing steam and the $(+)$ state $(1, T^b, u^b)$ containing water at boiling temperature. It has speed $v_{g,w}^b$ given by

$$v_{g,w}^b = v_{g,w}^b(S_w^b; u^b) = \frac{u^b}{\varphi}\frac{f_g^b(S_g^b)}{S_g^b} = \frac{u^b}{\varphi}\frac{1 - f_w^b(S_w^b)}{1 - S_w^b}. \tag{2.8}$$

Notice that, because $f_g(S_g = 0) = 0$ and $(\partial f_g/\partial S_g)(S_g = 0) = 0$ from Eq. (1.11) and from the quadratic behavior of the steam fractional flow function in the saturation given in Eq. (G.11), we obtain:

$$v_{g,w}^b(S_w = 1; u^b) = 0. \tag{2.9}$$

Similarly, for $S_w^b \leq S_{wc}$ from Eqs. (G.10) and (1.11),

$$v_{g,w}^b = \frac{u^b}{\varphi(1 - S_w^b)} > 0. \tag{2.10}$$

Remark 5. *It is easy to verify that v_s^b in Eq. (2.7) is monotone increasing in S_w^b when S_w^b is less than S^{infl}, the inflection abscissa of f_w, and decreasing when S_w^b is larger than S^{infl}.*

2.2. **Liquid water region.** We recall that the liquid water zone consists of the hot region, which is also part of the hot region examined in Section 2.1, and of the cold water zone.

In the liquid water zone there is no steam, so there is no mass transfer between steam and water. So $q = 0$. Also, in the liquid region $S_w = 1$, so Eqs. (2.3) and (2.4) reduce to

$$\varphi\frac{\partial \rho_w}{\partial t} + \frac{\partial(u\rho_w)}{\partial x} = 0, \tag{2.11}$$

$$\frac{\partial}{\partial t}\left(H_r + \varphi H_w\right) + \frac{\partial(uH_w)}{\partial x} = 0. \tag{2.12}$$

2.2.1. *Thermal rarefaction curves.* The characteristic speeds of the above equations are obtained by linearizing Eqs. (2.11), (2.12) relative to temperature variations at fixed pressure; we obtain the following equations where "prime" means differentiation relative to temperature:

$$\varphi\rho_w'\frac{\partial T}{\partial t} + u\rho_w'\frac{\partial T}{\partial x} + \rho_w\frac{\partial u}{\partial x} = 0 \tag{2.13}$$

$$\left(H_r' + \varphi H_w'\right)\frac{\partial T}{\partial t} + uH_w'\frac{\partial T}{\partial x} + H_w\frac{\partial u}{\partial x} = 0. \tag{2.14}$$

Dividing the first equation by ρ_w and the second one by H_w and subtracting we obtain a scalar transport equation for the temperature, whose characteristic speed is given by v_w

$$v_w = u\frac{C_w^p/H_w + \alpha_w}{\left(C_r^p + \varphi C_w^p\right)/H_w + \varphi\alpha_w}. \tag{2.15}$$

There is no other characteristic speed as it would be associated to velocity propagation with infinite speed.

At the rarefaction point $x/t = v_w$, we have

$$\frac{du}{dT} = v_w(C_r^p + \varphi C_w^p)/H_w - uC_w^p/H_w \tag{2.16}$$

Substitution of Equation 2.15 into Equation 2.16 leads after some algebraic manipulation to

$$\frac{du}{dT} = u\frac{C_r^p\alpha_w}{C_r^p + \varphi C_w^p + \varphi H_w\alpha_w} \tag{2.17}$$

This equation represents the thermal rarefaction curve in (u, T) space. Notice that if ρ_w does not depend on the temperature u is also independent of temperature, so u is constant. This situation is called a contact wave and will be considered further in the section.

2.2.2. *Thermal shock curves.* Let us consider a temperature discontinuity from T to T^0, with speed $v_w^{T,0}$ in the liquid water between the left state $(S_w = 1, T, u^0)$ and the right state $(S_w = 1, T = T^0, u^0)$. For such a *thermal water shock*, from Eqs. (2.11) and (2.12) one can obtain the following Rankine-Hugoniot relation, where we denote by u^0 the Darcy velocity in the liquid water region:

$$v_w^{T,0} = \frac{u^0\rho_w^0 - u\rho_w}{\varphi(\rho_w^0 - \rho_w)} = \frac{u^0H_w^0 - uH_w}{(H_r^0 + \varphi H_w^0) - (H_r + \varphi H_w)}, \tag{2.18}$$

where

$$H_w^0 = H_w(T^0), \quad H_r^0 = H_r(T^0), \quad \rho_w^0 = \rho_w(T^0).$$

We recall that all enthalpies vanish at T^0, so the Rankine-Hugoniot condition can be rewritten as

$$v_w^{T,0} = \frac{u^0\rho_w^0 - u\rho_w}{\varphi(\rho_w^0 - \rho_w)} = \frac{uH_w}{(H_r + \varphi H_w)}, \tag{2.19}$$

From the second equality in Eq. (2.19), we obtain that

$$u = \frac{H_r + \varphi H_w}{H_r\rho_w/\rho_w^0 + \varphi H_w}u^0, \tag{2.20}$$

which expresses the conservation of water mass.

The solution of this equation gives rise to a shock curve in (u, T) space, which provides the value of T at the left hand side of each point $x/t = v_w^{T,0}$.

From the last term in Eq. (2.19) and from Eq. (2.20):

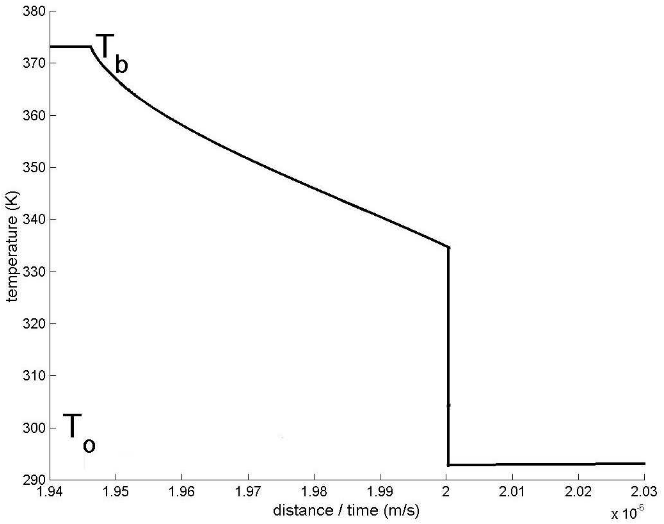

FIGURE 2.1. Cooling wave temperature profile in the liquid water region. Notice that it is very thin: $(2.00 - 1.94)/2.0 = 3\%$.

$$v_w^{T,0} = \frac{H_w}{H_r \rho_w / \rho_w^0 + \varphi H_w} u^0. \tag{2.21}$$

Thermal rarefaction waves and shock waves of the system 2.13 and 2.14 are adjacent forming a Buckley-Leverett like pattern illustrated in Figure 2.1. The adjacency state can be found by equating Eqs. (2.17), (2.20), (2.21) and the empirical expressions for $\rho_w(T)$ and for $H_w(T) = \int_{T^0}^{T} C_w^p(T)dT$.

2.2.3. *Contact cooling discontinuity.* For real water at pressures of the order of one atmosphere, $C_w^p(T)$ changes very little in the temperature range between ambient and boiling temperature so that the RHS of Equation 2.27 changes by about 3%. One can show that the result is that a wave group consisting of Buckley-Leverett-like sequence of thermal waves (a rarefaction and a shock) is formed in the water. Since its width is only 3% of the scale of interest, from now on we assume that $C_w^p(T)$ is constant. In this way the cooling wave group collapses into a contact discontinuity with zero width and the description of the Riemann solution is considerably shortened.

Let us consider a temperature discontinuity from T^b to T^0, with speed $v_w^{b,0}$ in the liquid water between the hot left state $(S_w = 1, T = T^b, u^b)$ and the cold right state $(S_w = 1, T = T^0, u^0)$. For such a *cooling contact discontinuity*, from Eqs. (2.11) and (2.12) one can obtain the following Rankine-Hugoniot relation, where we denote by u^b and u^0 the Darcy velocities at the discontinuity sides corresponding to T^b and T^0:

$$v_w^{b,0} = \frac{u^0 \rho_w^0 - u^b \rho_w^b}{\varphi(\rho_w^0 - \rho_w^b)} = \frac{u^0 H_w^0 - u^b H_w^b}{(H_r^0 + \varphi H_w^0) - (H_r^b + \varphi H_w^b)}, \tag{2.22}$$

where

$$H_w^b = H_w(T^b), \quad H_r^b = H_r(T^b), \quad \rho_w^b = \rho_w(T^b). \tag{2.23}$$

We recall that all enthalpies vanish at T^0, so the Rankine-Hugoniot condition can be rewritten as

$$v_w^{b,0} = \frac{u^0\rho_w^0 - u^b\rho_w^b}{\varphi(\rho_w^0 - \rho_w^b)} = u^b\frac{H_w^b}{H_r^b + \varphi H_w^b}. \tag{2.24}$$

From the second equality in Eq. (2.24), we obtain that

$$u^b = \frac{H_r^b + \varphi H_w^b}{H_r^b\rho_w^b/\rho_w^0 + \varphi H_w^b}u^0, \tag{2.25}$$

which expresses the conservation of water mass.

From the last term in Eq. (2.24) and from Eq. (2.25):

$$v_w^{b,0} = \frac{H_w^b}{H_r^b\rho_w^b/\rho_w^0 + \varphi H_w^b}u^0. \tag{2.26}$$

Remark 6. *Notice that the dependence of ρ_w on temperature is often small. If ρ_w were independent of temperature (constant), then Eq.* (2.25) *would imply that $u^b = u^0$.*

Remark 7. *Since all speeds in this problem scale with u, and u^{inj} is constant in time, u^0 and u^b are constant in time.*

Remark 8. *In the hot water zone, both $S_w = 1$ and $T = T^b$, so $q = 0$. Since the temperature is constant, so is ρ_w, thus Eq.* (2.11) *says that u is a constant, which has already been called u^b in Section 2.1. Equation* (2.12) *says that the characteristic speed (of temperature waves) in the hot water zone is*

$$v_w^b = \frac{C_w^p(T^b)}{C_r^p(T^b) + \varphi C_w^p(T^b)}u^b. \tag{2.27}$$

This is the propagation speed of small temperature perturbations near $T = T^b$ in the hot water zone.

2.3. **Steam condensation front.** This is a discontinuity joining a state $(-)$ containing steam and water at temperature T^b to pure water at temperature T^0, a state $(+)$; that is, it separates the hot steam zone from the cold water zone. It satisfies the following Rankine-Hugoniot conditions with speed v^{SCF} for Eqs. (2.3), (2.5) between states (S_w^b, T^b, u^b) and $(S_w^0 = 1, T^0, u^0)$. From the water balance (2.3) we obtain:

$$\begin{aligned} & u^b\left(\rho_w f_w + f_g\rho_g\right)^- - \varphi v^{SCF}\left(\rho_w S_w + S_g\rho_g\right)^- \\ = \quad & u^0\left(\rho_w f_w + f_g\rho_g\right)^+ - \varphi v^{SCF}\left(\rho_w S_w + S_g\rho_g\right)^+ \end{aligned} \tag{2.28}$$

and from the energy balance (2.5) we obtain:

$$\begin{aligned} & u^b\left(H_w f_w + H_g f_g\right)^- - v^{SCF}\left(H_r + \varphi H_w S_w + \varphi H_g S_g\right)^- \\ = \quad & u^0\left(H_w f_w + H_g f_g\right)^+ - v^{SCF}\left(H_r + \varphi H_w S_g + \varphi H_g S_g\right)^+. \end{aligned} \tag{2.29}$$

As no steam exists on the right of the SCF, we can say that $S_w^0 = f_w^0 = 1$ and $S_g^0 = f_g^0 = 0$ and thus Eq. (2.28) becomes

$$u^b\left(\rho_w f_w + \rho_g f_g\right)^- - \varphi v^{SCF}\left(\rho_w S_w + \rho_g S_g\right)^- = \rho_w^0\left(u^0 - \varphi v^{SCF}\right). \tag{2.30}$$

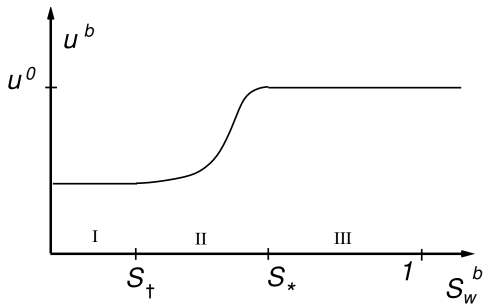

FIGURE 2.2. Speed u^b for fixed T^0, u^0, obtained from Eq. (2.35). The curve is almost horizontal at S_*; if ρ_g and H_g^B could be neglected, and ρ_w were independent of temperature, tangency would be exact (using Eq. (3.1)).

Under the same conditions we obtain for the heat balance equation (2.29):

$$\begin{aligned} u^b\left(H_w f_w + H_g f_g\right)^- &- v^{SCF}\left(H_r + \varphi H_w S_w + \varphi H_g S_g\right)^- \\ &= u^0 H_w^0 - v^{SCF}\left(H_r^0 + \varphi H_w^0\right) = 0. \end{aligned} \tag{2.31}$$

The RHS term of Eq. (2.31) vanishes in the absence of steam because of our convention for enthalpies, as far as rock and water are concerned. For the SCF velocity it follows from Eqs. (2.30), (2.31) that

$$u^0 = u^b\left(\frac{\rho_g^b}{\rho_w^0} f_g^b + \frac{\rho_w^b}{\rho_w^0} f_w^b\right) - \varphi v^{SCF}\left(\frac{\rho_g^b}{\rho_w^0} S_g^b + \frac{\rho_w^b}{\rho_w^0} S_w^b - 1\right), \tag{2.32}$$

$$v^{SCF} = u^b \frac{H_w^b f_w^b + H_g^B f_g^b}{H_r^b + \varphi H_w^b S_w^b + \varphi H_g^B S_g^b}, \tag{2.33}$$

where we used the nomenclature

$$H_g^B = H_g^s(T^b) + H_g^l = H_g^b + \Lambda^0 \rho_g^b. \tag{2.34}$$

Because $S_g^b = 1 - S_w^b$, $f_g^b = 1 - f_w^b$ and f_w^b depends only on the water saturation in the constant temperature steam zone, we observe that u^0 depends only on the water saturation and the Darcy velocity at the left of the SCF as well as on the velocity of the SCF.

From Eqs. (2.32) and (2.33), we can write u^0 in terms of u^b:

$$\frac{u^0}{u^b} = \left(\frac{\rho_w^b}{\rho_w^0} f_w^b + \frac{\rho_g^b}{\rho_w^0} f_g^b\right) - \varphi\left(\frac{\rho_w^b}{\rho_w^0} S_w^b + \frac{\rho_g^b}{\rho_w^0} S_g^b - 1\right)\frac{H_w^b f_w^b + H_g^B f_g^b}{H_r^b + \varphi H_w^b S_w^b + \varphi H_g^B S_g^b}. \tag{2.35}$$

Eqs. (2.33) and (2.35) represent the speeds v^{SCF} and u^0 in terms of u^b. Eq. (2.35) easily allows to read u^b in terms of u^0 (see Figure 2.2). We can use the expression of $\left[\frac{u^0}{u^b}\right]$ given by Eq. (2.35) in Eq. (2.33) to obtain v^{SCF} in terms of u^0:

$$v^{SCF} = u^0\left[\frac{u^0}{u^b}\right]^{-1}\frac{H_w^b f_w^b + H_g^B f_g^b}{H_r^b + \varphi H_w^b S_w^b + \varphi H_g^B S_g^b}. \tag{2.36}$$

Finally, we replace H_g^B in Eq. (2.36) by its definition given in Eq. (2.34).

Remark 9. *In principle, (+) states with temperature T different from T^0 could be considered, but because C_w^p was assumed to be constant such condensation discontinuities do not appear in the Riemann solution.*

2.4. **Cold water zone.** In the cold water zone, $S_w = 1$, so $q = 0$. Since $T = T^0$ is constant, so is ρ_w. Thus Eq. (2.11) says that u is a constant that has been called u^0. Equation (2.12) says that the characteristic speed (of temperature waves) in the cold water zone is

$$v^0 = \frac{C_w^p(T^0)}{C_r^p(T^0) + \varphi C_w^p(T^0)} u^0. \tag{2.37}$$

3. Wave bifurcation analysis

Let us consider the situation where the hot steam zone is followed by a cold water zone. For such a situation to occur, there must be a steam condensation discontinuity in between. Let us first examine the critical case $(*)$ when the speed of the condensation discontinuity is the same as the characteristic speed in the cold water zone.

3.1. **The hot-cold bifurcation.** Because speed equality of different waves typically represents resonance and generates bifurcations, let us consider the case when the SCF speed is so large that it equals the cooling contact discontinuity speed. We expect this bifurcation to represent the boundary between configurations containing either SCF shocks or cooling discontinuities. Equating the cooling discontinuity speed $v_w^{b,0}$ (from Eq. (2.24) or equivalently from (2.26)) with v^{SCF} given by Eq. (2.36). Using Eq. (2.8), we conclude that we have the following remarkable speed equalities.

Theorem 1. *Fix T^0 and T^b (or equivalently T^0 and the reservoir pressure). Consider the following three shocks: $HISW$ shock between (S_w^b, T^b, u^b), $(1, T^b, u^b)$, cooling shock between $(1, T^b, u^b)$, $(1, T^0, u^0)$, SCF between (S_w^b, T^b, u^b), (S_w^0, T^0, u^0). If any <u>two</u> of their wave speeds coincide at a certain $S_w^b = S_*$, then their <u>three</u> speeds coincide at this S_*.*

Proof. The proof consists of three parts. The velocities are given in Eqs. (2.8), (2.19) and (2.33).

(1) Assume that at $S_w^b = S_*$ we have $v_{g,w}^b = v_w^{b,0}$.

From the equality in speeds, Eqs. (2.8) and Eqs. (2.24) we have for $S_g^b = 1 - S_*$:

$$\frac{u^b}{\varphi}\frac{f_g^b}{S_g^b} = \frac{u^b}{\varphi}\frac{1-f_w^b}{1-S_w^b} = u^b\frac{H_w^b}{H_r^b + \varphi H_w^b}. \tag{3.1}$$

Multiplying numerator and denominator of the second fraction in Eq. (3.1) by H_w^b and subtracting the results to the corresponding terms in the third fraction, we obtain:

$$\frac{u^b}{\varphi}\frac{f_g^b}{S_g^b} = u^b\frac{H_w^b f_w^b}{H_r^b + \varphi H_w^b S_g^b}. \tag{3.2}$$

Multiplying numerator and denominator of the first fraction in Eq. (3.2) by H_g^B and adding the results to the corresponding terms in the second equation, we obtain:

$$\frac{u^b}{\varphi}\frac{f_g^b}{S_g^b} = u^b\frac{H_w^b f_w^b + H_g^B f_g^b}{H_r^b + \varphi H_w^b S_w^b + \varphi H_g^B S_g^b}. \tag{3.3}$$

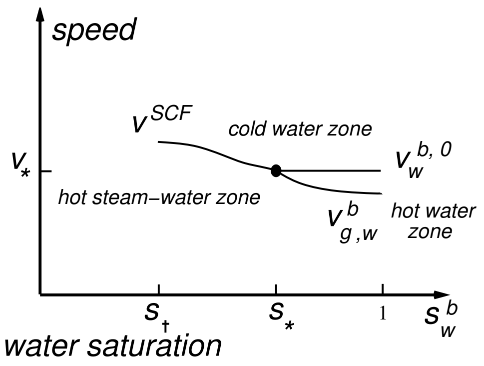

FIGURE 3.1. Schematic bifurcation diagram near S_* (for fixed u^0, T^0) versus S_w^b, the saturation on the left of the $HISW$ shock or of the SCF.

From Eqs. (2.8) and (2.33), we see that $v_{g,w}^b = v^{SCF}$.

(2) Performing the above calculation in reverse order, we can prove that $v_{g,w}^b = v^{SCF}$ implies $v_{g,w}^b = v^{SCF} = v_w^{b,0}$.

(3) Assume that at S_* we have $v_w^{b,0} = v^{SCF}$.

From Eqs. (2.26) and (2.33), and assuming that $\rho_w^b = \rho_w^0$, i.e. the density of water is independent of temperature,

$$v_w^{b,0} = u^b \frac{H_w^b}{H_r^b + \varphi H_w^b} = u^b \frac{H_w^b f_w^b + H_g^B f_g^b}{H_r^b + \varphi H_w^b S_w^b + \varphi H_g^B S_g^b}. \tag{3.4}$$

Substituting $f_w^b = 1 - f_g^b$, $S_w^b = 1 - S_g^b$ in the numerator and denominator of the last fraction in Eq. (3.4) we obtain:

$$v_w^{b,0} = u^b \frac{H_w^b}{H_r^b + \varphi H_w^b} = u^b \frac{H_w^b - H_w^b f_g^b + H_g^B f_g^b}{H_r^b + \varphi H_w^b - \varphi H_w^b S_g^b + \varphi H_g^B S_g^b}. \tag{3.5}$$

Subtracting the numerator and denominator of the first fraction from the corresponding terms in the last fraction we obtain:

$$v_w^{b,0} = \frac{u^b}{\varphi} \frac{f_g^b(-H_w^b + H_g^B)}{S_g^b(-H_w^b + H_g^B)}, \tag{3.6}$$

or, from Eq. (2.8), $v_w^{b,0} = v_{g,w}^b$, and the proof is complete.

□

The speed $v_{g,w}^b$ is the Buckley-Leverett speed of propagation of a hot steam shock from S_w^b to $S_w = 1$ (pure hot water, or no steam) governed by Eq. (2.6). Thus, each pair of states of this one-parameter family of discontinuities (S_*, T^b, u^b), $(1, T^0, u^0)$ acts as an organizing center in the space of all solutions of the Riemann problem; the first member (S_*, T^b, u^b) of each such pair is denoted by $*$. This family of discontinuities is parameterized by u^0 for instance, as explained in Remark 2.

Theorem 1 provides information related to the structure at the left of the temperature discontinuities. In Figure 3.1, S_* corresponds to the saturation of a state $*$. The $*$ state separates two different configurations; in one of them, there is a hot steam zone and a cold

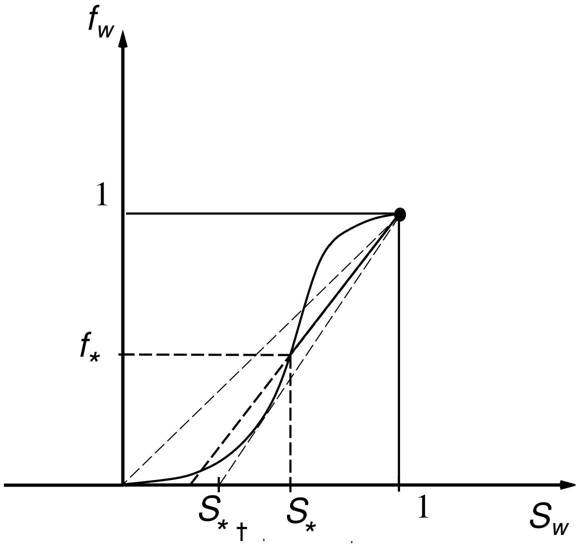

FIGURE 3.2. Finding S_* from second equality in Eq. (3.1), by a solid line with slope $\varphi H_w^b/(H_r^b+\varphi H_w^b)$; dashed bounding lines through $(0,0)$ and $(S_{*\dagger},0)$.

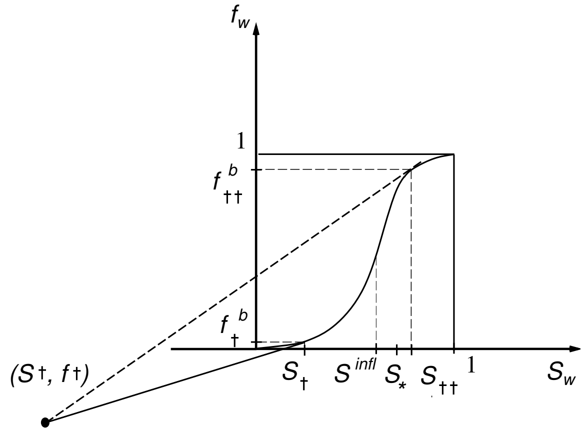

FIGURE 3.3. Graphical solution of Eqs. (3.7) and (2.33) for steam-water bifurcation. The solid line represents the SCF shock

water zone separated by a SCF, while in the other there is a hot steam zone, a hot water zone and a cold water zone.

3.2. **The steam-water bifurcation.** Let us fix T^0 and T^b (or equivalently T^0 and the reservoir pressure). Let us now examine the critical case ($\dagger$) when the speed of the steam condensation discontinuity is so high that it becomes the same as the characteristic speed of saturation waves in the hot region given in Eq. (2.7), so the SCF overtakes the cooling discontinuity. One can expect that the SCF cannot exist with higher speed. At $S_\dagger$, the SCF becomes a left-contact. At such a state $(S,T,u)=(S_\dagger,T^b,u^b)$, we have:

$$v_s^b(S_\dagger; u^b) \equiv \frac{u^b}{\varphi}\frac{\partial f_w^b}{\partial S_w}(S_\dagger) = v^{SCF}. \tag{3.7}$$

It is easy to find numerically or graphically (see Fig. 3.3) the solution of Eq. (3.7) using Eq. (2.33) and solve for $S_\dagger$. Notice that u^b cancels out. Subsequently we can use Equation (2.35) to calculate the downstream velocity u^0 in terms of v^{SCF}. Equivalently, we can use Eqs. (2.35), (2.36) to obtain u^b and v^{SCF} in terms of u^0.

Remark 10. *If Figure 3.3 were drawn to scale for the actual data nothing would be visible. The drawing is for illustrative purposes. In the numerical example studied in detail, we find the following values:* $S^\dagger = -1.32449$, $f^\dagger = -0.00471$, $S^{infl} = 0.884747$, $S_\dagger = 0.308042$, $S_{\dagger\dagger} = 0.991435$, *and* $S_* = 0.983167$.

Equating v^{SCF} given by Eq. (3.7) with Eq. (2.33), making $f_g^b = 1 - f_w^b$, $S_g = 1 - S_w$, we obtain

$$\frac{\partial f_w^b}{\partial S_w}(S_\dagger) = \frac{f_w^b(S_\dagger) - f^\dagger}{S_\dagger - S^\dagger}, \tag{3.8}$$

where

$$S^\dagger = \frac{H_r^b/\varphi + H_g^B}{H_g^B - H_w^b}, \qquad f^\dagger = \frac{-H_g^B}{H_g^B - H_w^b}, \tag{3.9}$$

and all quantities are evaluated at the boiling temperature T^b. The physics of water at normal pressure dictates that at the boiling temperature, $H_g^B > H_w^b$, thus $S^\dagger < 0$ and

$$f^\dagger = \frac{-H_r^b/\varphi}{H_g^B - H_w^b} + S^\dagger < S^\dagger < 0. \tag{3.10}$$

Remark 11. *Since for steam–water* $(S^\dagger, T^\dagger)$ *satisfies the inequalities* (3.10), *there is another solution point* $(S_{\dagger\dagger}, f_{\dagger\dagger}^b)$ *for Eq. (3.7) closer to (1,1) as shown in Fig. 3.3. However, it does not play any role in the Riemann solution of the current problem because it exceeds* S_*, *according to Remark 10.*

The contact bifurcation $S_\dagger$ *separates different wave structures in the steam-water zone as can be seen in Fig. 3.4.*

In Figures 4.5 and 2.2, we show the characteristic speed v^{SCF} and u^b for each S_w^b, at temperature T^b for fixed u^0. As we shall see in Section 4.2, the diagram in Fig. 4.5 determines the structure of the Riemann solution in the steam zone.

Remark 12. *By inspection of Figure 3.3, we see that slightly above and below* $S_\dagger$ *there exist* S_+ *and* S_- *with* $v^{SCF}(S_+) = v^{SCF}(S_-)$ *larger than* $v^{SCF}(S_\dagger)$ *such that*

$$(S_+ - S_\dagger)v^{SCF}(S_+) = \frac{u^b}{\varphi}(f_w^b(S_+) - f_\dagger)$$

$$(S_- - S_\dagger)v^{SCF}(S_-) = \frac{u^b}{\varphi}(f_w^b(S_-) - f_\dagger)$$

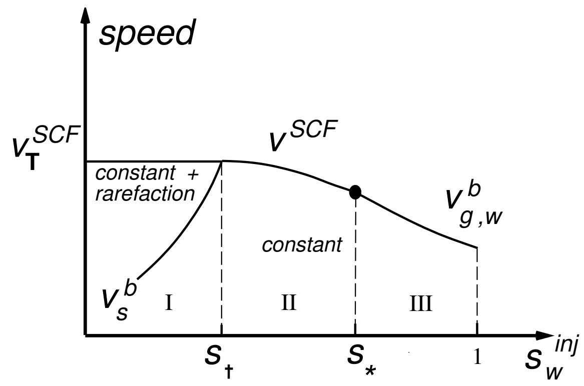

FIGURE 3.4. Structure of the steam-water zone below solid curve marked by v_s^b, v_T^{SCF}, v^{SCF}, $v_{g,w}^b$. given in equation (2.7), (2.33) with S_w=$S_\dagger$,equation (2.33) with $S_\dagger < S_w^{inj} < S_*$, and equation (2.8) respectively. The figure is not drawn to scale.

Subtracting these two equations, dividing by $(S_+ - S_-)$ and taking the limit as $S_+, S_- \to S_\dagger$ we recover that

$$\frac{u^b}{\varphi}\frac{\partial f_w^b}{\partial S_w}(S_\dagger) = v^{SCF}, \tag{3.11}$$

and obtain that $S_\dagger$ maximizes v^{SCF}, as illustrated in Figures 3.1, 3.4 and 4.5. An analogous argument holds at $S_{\dagger\dagger}$.

Remark 13. *The SCF shocks are represented in Figure 3.3 as segments with slope v^{SCF}/u^b between $(S^\dagger, f^\dagger)$ and (S, f) for $0 \le S \le S_\dagger$. We see that as S increases v^{SCF} decreases and the shock amplitude $S - S^\dagger$ increases.*

Remark 14. *We have shown that v^{SCF}/u^b has an extremum at $S_\dagger$; the Figure 3.3 shows that this slope has an extremum at $S_\dagger$. Thus u^b also has an extremum at $S_\dagger$.*

3.3. **Waves in the liquid water region.** Because the initial reservoir temperature is T^0, the liquid water region must always contain a cold water zone at temperature T^0 far away from the place where hot steam is injected. If the liquid water region receives water at temperature T^b from the steam zone, the liquid water region consists of a hot liquid water zone at temperature T^b and a cold water zone at temperature T^0, separated by a cooling discontinuity that moves with speed $v_w^{b,0}$ given by Eq. (2.26). This cooling discontinuity exists provided $v_w^{b,0} > v_{g,w}^b$ from Eq. (2.8) i.e. the hot isothermal steam-water shock velocity ($HISW$). In this case the $HISW$ shock at which the steam saturation becomes zero and the cooling shock where the temperature jumps to the ambient temperature are separated. See region $S > S_*$ in Fig. 3.1.

On the other hand, if $v_w^{b,0} > v_{g,w}^b$ were to be violated, there would be no hot water zone and no cooling discontinuity. See region $S < S_*$ in Fig. 3.1, where there is a steam condensation front instead of a cooling discontinuity.

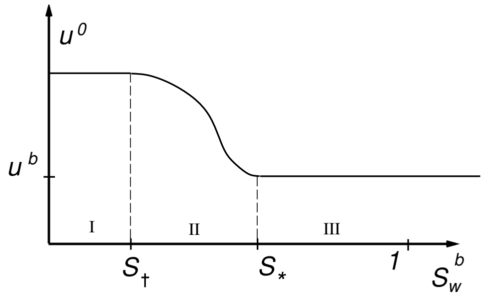

FIGURE 4.1. Speed u^0 for fixed T^b, u^{inj}, obtained from Eq. (4.1) and Fig. 2.2.

3.4. **Waves in the hot steam zone.** The waves in this zone can be found by a pure Buckley-Leverett analysis of Eq. (2.6), with one *caveat*. In the sequence of zones starting at the injection well, the first zone is a steam zone, and the last one is a cold water zone, with heat flow governed by the system (2.11)–(2.12). The cold water zone is reached either via a steam condensation shock or via a cooling shock. In the latter case, if there is no other shock between the steam zone and the cold water zone, all waves in the steam zone must have speeds that do not exceed the cooling shock speed $v_w^{b,0}$ given by Eq. (2.25). In particular, if there is a $HISW$ shock with speed given by $v_{g,w}^b$ in Eq. (2.8), we must have $v_{g,w}^b \leq v_w^{b,0}$. Similarly, if there is a saturation rarefaction wave with speed given by v_s^b in Eq. (2.7), we must have $v_s^b \leq v_w^{b,0}$, the cooling contact discontinuity velocity.

Because of Theorem 1, we see that the restrictions above are satisfied precisely for saturation S_w^b in the hot water zone with values between $[S_*, 1]$, see Figure 4.5. For steam–water at the conditions considered in this work, one can verify that the steam water bifurcation water saturation $S_\dagger$ is smaller than S_* in Fig. 3.3. Because $S_\dagger < S_*$, there are no Buckley-Leverett shocks between $[S_{wc}, S_*]$. This is so because below $S_\dagger$ there are no shocks as rarefaction wave velocities increase monotonically from S_{wc} to $S_\dagger$. At $S_\dagger$ the velocity is equal to the SCF velocity. Between $S_\dagger$ and S_* there are no shocks as the rarefaction wave velocities are larger than the SCF velocity.

Another case of interest occurs if steam of 100% quality is injected, *i.e.* $S_w = S_{wc}$, the connate water saturation. In this case, a saturation rarefaction wave starts at $x = 0$ in the steam zone. A mixture of steam and water can also be injected. As long as $S_w^{inj} < S_\dagger$, at $x = 0$ there is a constant state followed by a saturation rarefaction wave. Of course, in the Buckley-Leverett solution for the steam zone the rarefaction wave containing a saturation value S_w satisfies the geometric compatibility condition:

$$\frac{u^{inj}}{\varphi}\frac{\partial f_w^b(S_w)}{\partial S_w} \leq v^{SCF}. \tag{3.12}$$

4. CONSTRUCTION OF THE RIEMANN SOLUTION

Here we describe a systematic way of constructing the Riemann solution through a *wave curve*. Then we summarize the resulting Riemann solution.

4.1. **The wave curve.** Let us fix the initial state of the reservoir as $S_w^0 = 1, T = T^0, u = u^0$, which is necessarily the rightmost constant state in the Riemann solution. It turns out to be convenient for the discussion to imagine that an arbitrary value for u_0 has been specified. Let us decrease the injection saturation S_w^{inj} (at the boiling temperature) from $S_w = 1$ to

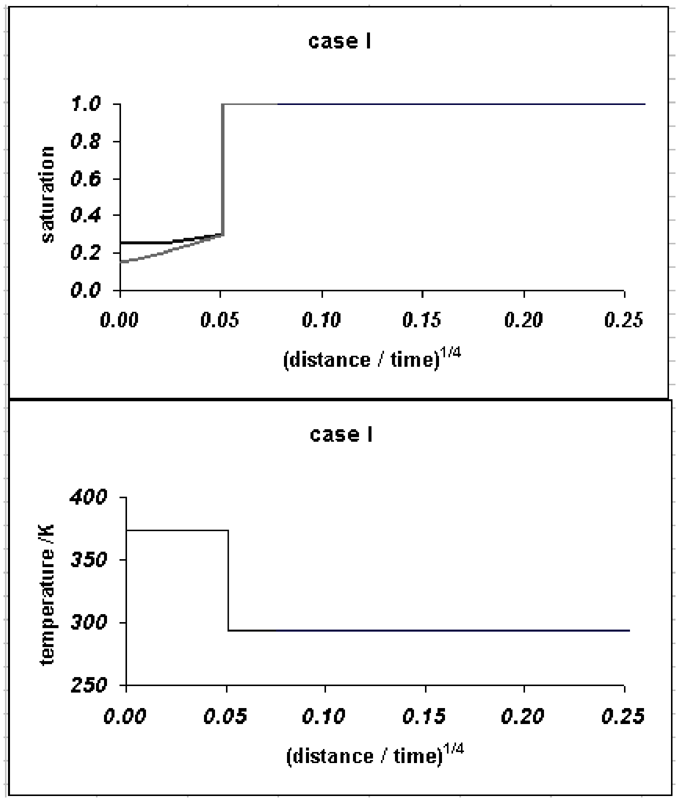

FIGURE 4.2. Two cases of steam injection: at connate water saturation S_{wc} or at a low water saturation. With injection at S_{wc} there is a rarefaction wave and a SCF. With injection of low water saturation above S_{wc} there is a constant state before the rarefaction.

$S_w = S_{wc}$; in our case this corresponds to changing S_w^b, the water saturation at the $HISW$ shock with speed given in Eq. (2.8). For each S_w^{inj}, we construct the sequence of elementary waves (and constant states) with decreasing speeds from right to left, that is from S^0 to S_w^b. There is a constant state to the left of S_w^b, so there is no other wave to the left of S_w^b, the steam shock. For each S_w^b, we mark its wave speed, forming the solid curves in Fig. 4.5. This sequence, parameterized by S_w^b, is called a *backward wave curve* from $(S_w = 1, T^0, u^0)$. It combines all information needed for describing the structure of the Riemann solution, and for verifying necessary speed relations for the admissibility of the shocks involved. On rarefaction segments of this wave curve, the characteristic speed decreases, while on shock segments of this wave curve, the shock speed increases [11],[23]. We refer to Fig. 4.5.

When S_w^{inj} lies between S_* and 1, the wave with fastest possible speed is the cooling shock in the liquid water region (see Section 3.4), so the backward wave curve corresponds to such a shock wave, with speed given by $v_w^{b,0}$ in Eq. (2.26). There is a hot steam-water region and a cold water zone. In the hot steam-water region, generically there is a Buckley-Leverett rarefaction-shock and a constant state. The hot steam-water region terminates with the $HISW$ shock.

The analysis from now on relies on the fact that for steam–water in the actual reservoir, $S^{infl} < S_*$. For S_w^{inj} within $(S_\dagger, S_*)$, the wave with slowest speed is the SCF, with speed v^{SCF}. At the left of the SCF, characteristic speed v_s^b exceeds v^{SCF}, so there can be no

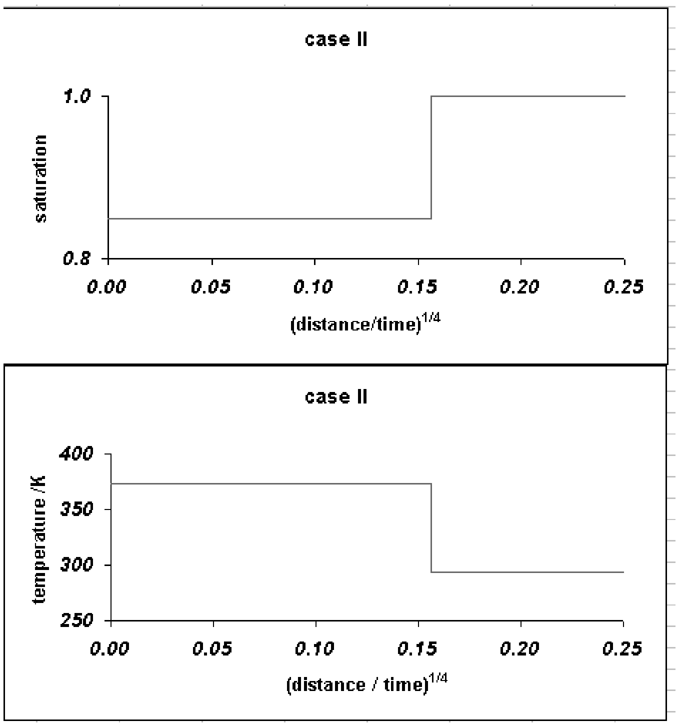

FIGURE 4.3. Steam injection at intermediate water saturation. We get a constant state upstream and the steam condensation front. The SCF moves faster than in Figure 4.2

rarefactions nor shocks to the left of the SCF. Thus, for S_w^{inj} in such range, the solution (from left to right) consists of a constant state of steam and water at temperature T^b, a SCF jumping from S_w^{inj} to S_*, and a constant cold water zone.

Recall that $S_\dagger < S^{infl}$. Therefore, from S_w^{inj} within $(S_{wc}, S_\dagger)$, the slowest speed is a hot steam–water rarefaction speed v_s^b, which is smaller than v^{SCF} (v_s^b and v^{SCF} coincide at the left state $S_\dagger$), so there are rarefactions to the left of the SCF. Thus the solution consists of a constant state with saturation S_w^{inj} as in the previous case (this constant state disappears if $S_w^{inj} = S_{wc}$), a rarefaction wave from S_w^{inj} to $S_\dagger$, a SCF from $S_\dagger$ to S_*, and a constant cold water zone.

Let us explain how the Darcy velocity u^b is constructed for each value of S_w^{inj}. If S_w^{inj} lies in the interval $(S_*, 1)$, u^b is given by Eq. (2.25), and the speed $v_w^{b,0}$ of the cooling shock is given by Eq. (2.26) (Case *III*). (As explained in Section 2.1, the velocity u is constant in the hot region and equals u^b.) If S_w^{inj} lies in the interval $S_\dagger$ and S_*, u^b is given by Eq. (2.35). The speed of the SCF is given by Eq. (2.36), (Case *II*).

If S_w^{inj} lies in the interval $(S_{wc}, S_\dagger)$ (Case *I*), since u^b has to match at the boundary of Cases *I* and *II*, u^b is given by Eq. (2.36) with S_w replaced by $S_\dagger$. Thus u^b is independent of S_w^{inj} in Case *I*.

A summary of the behavior of $u^b(S_w^{inj})$ is presented in Fig. 2.2. Here $u^b(S_w^{inj})$ is the value of u^b calculated in the previous paragraphs for a fixed u^0.

We are ready to abandon the assumption that u^0 is known. This is impractical, since normally one specifies u^{inj} rather than u^0. We take advantage of the fact that all speeds are

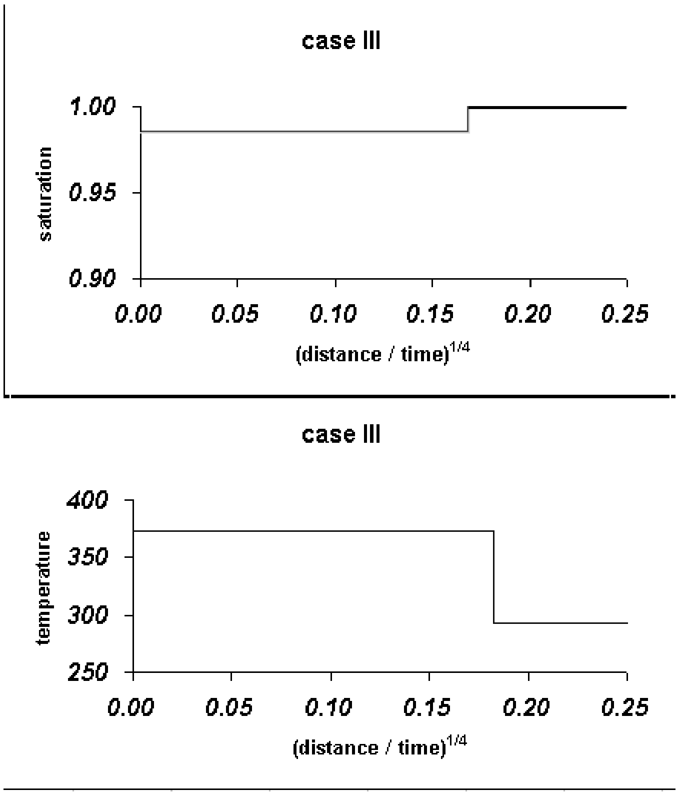

FIGURE 4.4. Steam injection at a high water saturation. We get a constant state upstream, the Buckley-Leverett-saturation shock and the cooling discontinuity. These two waves have distinct speeds; they are both faster than the SCF in Figure 4.3

proportional to find the actual speed in the cold water zone $u^0(S_w^{inj})$ for specified u^{inj}, as follows:

$$\frac{u^b(S_w^{inj})}{u^0} = \frac{u^{inj}}{u^0(S_w^{inj})}. \tag{4.1}$$

From this equation we recover $u^0(S_w^{inj})$, essentially by inverting the variable represented in the ordinate in Fig. 2.2. Thus we obtain Fig 4.1.

4.2. **Summary of the Riemann solution.** The solution consists of three parts, *viz.* a hot region (A) at constant boiling temperature, an infinitesimally thin cooling front (B) or discontinuity, where all possible steam condensation occurs, and a cold liquid water region downstream (C). See Figure 1.1.

As we have seen, the nature of the solution changes and there are three possible cases (I), (II), and (III), depending on the injected steam quality $S_g^{inj} = 1 - S_w^{inj}$. Cases ($II$) and ($III$) are separated by the hot-cold bifurcation, while Cases (I) and (II) are separated by the steam-water bifurcation.

Case (I) occurs when the saturation wave velocity $v_s^b(S_w^{inj}; u^{inj}) \leq v^{SCF}$ (see Eq. (2.7)); it consists of a sequence of a constant state at the injection end, a *rarefaction wave* in the

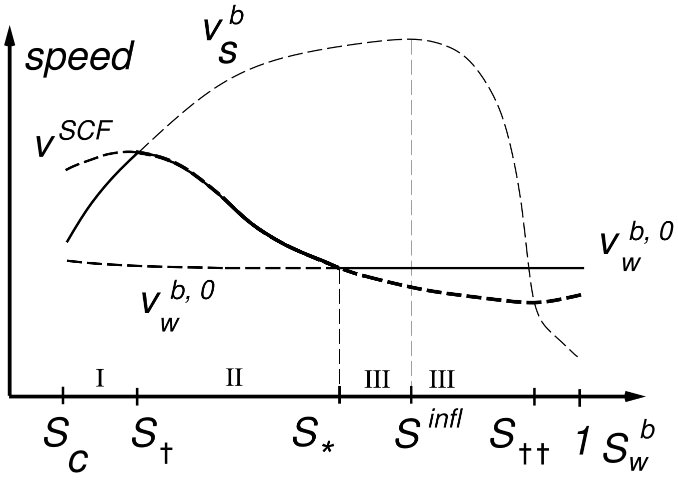

FIGURE 4.5. Wave speed diagram for left states (S_w^b, T^b, u^b) reachable from the right state $(1, T^0, u^0)$; for this right state the curve marked v^{SCF} is the Rankine-Hugoniot curve projected onto the (S_w, v) plane. The velocity of the SCF is v^{SCF} (Eq. (2.33)), v_s^b is the hot region saturation characteristic speed (Eq. (2.7)), and $v_w^{b,0}$ is the velocity of the cooling contact discontinuity (Eq. (2.26))

hot steam zone (A) ending with saturation $S_\dagger$ at the SCF (B) with speed v^{SCF} defined by saturations $S_\dagger$ and $S_w = 1$, and a cold water constant state in (C). The constant state in (A) disappears if the injection saturation is S_{wc}. See Fig. 4.2. The rarefaction disappears in case of equality rather than strict inequality, $v_s^b(S_w^{inj}; u^{inj}) = v^{SCF}$, as in this case $S_w^{inj} = S_\dagger$.

Case (*II*) occurs for $v_{g,w}^b(S_w^{inj}, u^{inj}) < v^{SCF} < v_s^b(S_w^{inj}; u^{inj})$; see Eqs. (2.7), (2.8) and (2.9). This case consists of a hot constant steam–water state in (A), the SCF (B) with speed v^{SCF} defined by left and right saturations S_w^{inj} and 1 (see Eq. (2.36)), and a constant cold water state in (C). See Fig. 4.3.

Case (*III*) occurs for a typically small region for the cooling contact discontinuity velocity $v_w^{b,0}$ (given in Eq. (2.26)) with $v_w^{b,0} > v_{g,w}^b(S_w^{inj}, u^{inj})$ (see Eq. (2.8)), i.e. the hot isothermal steam-water shock velocity. In this case, there is no SCF. In the hot region (A) there is a constant state with steam-water, then another constant state of pure hot water at the same boiling temperature, separated by a Buckley-Leverett shock. Then there is a cooling shock with speed $v_w^{b,0}$, where the saturation of water is constant ($S_w = 1$) and the temperature changes from T^b to the reservoir temperature T^0. See Fig. 4.4.

Figure 3.4 illustrates the saturation dependence of the various velocities that are the basis of the steam-water zone structure, for Cases (*I*), (*II*), (*III*).

5. LAX CONDITIONS FOR THE STEAM CONDENSATION FRONT

Despite the fact that our system does not satisfy Lax's theorem hypotheses, we will compare the SCF speed to the left and right characteristic speeds. We will conclude that from the point of view of Lax's inequalities, the SCF is a 2-shock or a limit of such shocks.

We introduce the heat capacities $C_p(T)$ as the derivatives of the enthalpies [J/m^3] at constant pressure, *i.e.* $C_w^p(T)$ is the heat capacity of water and $C_g^p(T)$ is the heat capacity of steam. In the same way we define the thermal expansivity of water and steam $\alpha_w(T)$ and $\alpha_g(T)$ as minus the temperature derivative of the density divided by the density (see Appendix G).

Eqs. (2.3)–(2.4) may be written in quasilinear form as:

$$-\frac{\partial u}{\partial x}(\rho_w f_w + \rho_g f_g) = -\varphi\Big[(S_w\rho_w\alpha_w + S_g\rho_g\alpha_g)\frac{\partial T}{\partial t} + \big(\rho_g - \rho_w\big)\frac{\partial S_w}{\partial t}\Big]$$

$$-u\Big[\,\big(f_w\rho_w\alpha_w + f_g\rho_g\alpha_g + \big(\rho_g - \rho_w\big)\partial f_w/\partial T\big)\,\frac{\partial T}{\partial x} - \bigg((\rho_w - \rho_g)\frac{\partial f_w}{\partial S_w}\bigg)\frac{\partial S_w}{\partial x}\Big], \tag{5.1}$$

$$q\Lambda^0 - \frac{\partial u}{\partial x}(H_w f_w + H_g^s f_g) = \varphi\Big[\big(\frac{C_r^p}{\varphi} + S_w C_w^p + S_g C_g^p\big)\frac{\partial T}{\partial t} + \big(H_w - H_g^s\big)\frac{\partial S_w}{\partial t}\Big]$$

$$+u\Big[\big(f_w C_w^p + f_g C_g^p + (H_w - H_g^s)\partial f_w/\partial T\big)\frac{\partial T}{\partial x} + \bigg((H_w - H_g^s)\frac{\partial f_w}{\partial S_w}\bigg)\frac{\partial S_w}{\partial x}\Big]. \tag{5.2}$$

We restrict our attention to regions where $\partial u/\partial x = 0$ and $\Lambda = 0$, that is, away from any kind of shocks. Thus, the LHS terms of Eqs. (5.1), (5.2) vanish.

We let

$$A_I = \frac{C_r^p}{\varphi} + S_w C_w^p + S_g C_g^p, \qquad A_{II} = f_w C_w^p + f_g C_g^p + (H_w - H_g^s)\partial f_w/\partial T. \tag{5.3}$$

Multiplying the RHS of Eq. (5.1) by $-(H_w - H_g^s)$ and of Eq. (5.2) by $(\rho_w - \rho_g)$ and adding leads to a new equation, which will be used instead of Eq. (5.2):

$$\varphi\Big[(H_w - H_g^s)(S_w\rho_w\alpha_w + S_g\rho_g\alpha_g) + (\rho_w - \rho_g)\,A_I\Big]\frac{\partial T}{\partial t}$$

$$+u\Big[(H_w - H_g^s)\Big(f_w\rho_w\alpha_w + f_g\rho_g\alpha_g + (\rho_g - \rho_w)\partial f_w/\partial T\Big) + (\rho_w - \rho_g)A_{II}\Big]\frac{\partial T}{\partial x} = 0. \tag{5.4}$$

We let

$$A_{III} = \big(H_w - H_g^s\big)\,(S_w\rho_w\alpha_w + S_g\rho_g\alpha_g) + (\rho_w - \rho_g)\,A_I, \tag{5.5}$$

$$A_{IV} = \Big(\,\big(H_w - H_g^s\big)\,(f_w\rho_w\alpha_w + f_g\rho_g\alpha_g + (\rho_g - \rho_w)\partial f_w/\partial T) + (\rho_w - \rho_g)\,A_{II}\Big). \tag{5.6}$$

Thus in regions where $\partial u/\partial x = 0$ and $\Lambda = 0$, that is, away from any kind of shocks (see Remarks 1 and 4), Eqs. (5.1)–(5.4) may be written in matrix form as:

$$\left(A\frac{\partial}{\partial t} + B\frac{\partial}{\partial x}\right)\begin{pmatrix} S \\ T \end{pmatrix} = 0. \tag{5.7}$$

Let μ be a characteristic speed. Then the determinant of the following matrix must vanish:

$$-\mu\varphi\begin{pmatrix}(\rho_g-\rho_w) & (S_w\rho_w\alpha_w+S_g\rho_g\alpha_g)\\ 0 & A_{III}\end{pmatrix}$$
$$+u\begin{pmatrix}(\rho_g-\rho_w)\,\partial f_w/\partial S_w & f_w\rho_w\alpha_w+f_g\rho_g\alpha_g+(\rho_g-\rho_w)(\partial f_w/\partial T)\\ 0 & A_{IV}\end{pmatrix}. \tag{5.8}$$

Since the matrix above is upper triangular, the characteristic speeds are easily read from the diagonals:

$$\mu=\frac{u}{\varphi}\frac{\partial f_w}{\partial S_w}\qquad\text{and}\qquad\mu=\frac{u}{\varphi}\frac{A_{IV}}{A_{III}}. \tag{5.9}$$

(It is easy to check that A_{III} never vanishes.)

Now, in the liquid water region on the right of the SCF, $S_g=0$, $f_g=0$, $\frac{\partial f_w}{\partial S_w}=0$, the characteristic speeds are

$$\mu=0\qquad\text{and}\qquad v^0=\frac{C_w^p(T^0)}{C_r^p(T^0)+\varphi C_w^p(T^0)}u^0. \tag{5.10}$$

The latter speed has already been calculated in Eq. (2.37).

On the other hand, in the hot steam zone the characteristic speeds are

$$v_s^b=\frac{u^b}{\varphi}\frac{\partial f_w^b}{\partial S_w},\qquad\text{and}\qquad v_T^b=\frac{u^b}{\varphi}\frac{A_{IV}(T^b)}{A_{III}(T^b)}. \tag{5.11}$$

The first speed has already been calculated in Eq. (2.7). The second speed of thermal waves is shown in Figure 4.5 as a function of S_w at $T=T^b$.

For a $(-)$ state for the SCF with S_w in $(S_*,S_\dagger)$ we have that the thermal characteristic speed in the steam zone satisfies $0<v^0<v^{SCF}$, and the steamfront velocity satisfies $v_T^b<v^{SCF}<v_s^b$, so the SCF would be called a 2-shock in Lax's classification scheme. However, Lax's theorem only applies to shocks with small amplitude, while the SCF is a large shock, and only if the governing equations were a system of conservation laws satisfying appropriate technical hypotheses, such as genuine nonlinearity, which is actually violated at the inflection S^{infl}. Moreover, even the Lax inequalities are violated starting at the steam-water bifurcation; there is no conclusive mathematical evidence that the SCF shock needed to complete the Riemann solution is physically admissible. This is the issue resolved in the appendices.

6. Summary and conclusions

There are two main results in this work. The first one is a complete and systematic description of all possible solutions of the Riemann problem for the injection of a mixture of steam and water into a water-saturated porous medium, for all possible reservoir temperatures and pressures.

The second result is that the regularization of the equations using capillary pressure and a non-equilibrium kinetic equation in the steam condensation zone gives consistent result, providing strong mathematical evidence that this is the correct regularization for the steam injection problem in porous media.

Acknowledgments: This work was partially done at IMA, University of Minnesota, and therefore partially funded by NSF. We also thank Beata Gundelach for careful and expert typesetting of this paper.

Appendix A. Blow up of the steam condensation zone

In this section, we assume that time and distance have been scaled so that the diffusion terms and the heat condensation terms balance, so that the Steam Condensation Zone has width $O(1)$; it will be studied as a travelling wave extending from $-\infty$ to $+\infty$. In the steam condensation zone capillary pressure effects, conduction, as well as mass and heat transfer terms have all to be taken into account. However, because this zone is thin relative to the zone spanned by the whole, we are always justified in ignoring pressure variation effects on densities within the zone.

For the analysis of travelling waves, it is advantageous to define the cumulative condensation distribution $Q(x,t)$ and cumulative condensation $Q^+(t)$ by

$$Q(x,t) = \int_{-\infty}^{x} q(x',t)dx', \qquad Q^+(t) = \int_{-\infty}^{+\infty} q(x',t)dx'. \tag{A.1}$$

Let us assume that all quantities depend only on $\xi = x - v^{SCF}t$. Now equations (1.14) – (1.16) and (A.1) can be written as

$$-\varphi v^{SCF}\frac{d\left(\rho_w S_w\right)}{d\xi} + \frac{d\left(\rho_w u f_w\right)}{d\xi} = \frac{dQ}{d\xi} + \frac{d}{d\xi}\left(\rho_w \Omega \frac{dS_w}{d\xi}\right), \tag{A.2}$$

$$-\varphi v^{SCF}\frac{d\left(\rho_g S_g\right)}{d\xi} + \frac{d\left(\rho_g u f_g\right)}{d\xi} = -\frac{dQ}{d\xi} - \frac{d}{d\xi}\left(\rho_g \Omega \frac{dS_w}{d\xi}\right), \tag{A.3}$$

$$\begin{aligned} -v^{SCF}\frac{d}{d\xi}\left(H_r + \varphi H_w S_w + \varphi H_g^s S_g\right) + \frac{d}{d\xi}\left(u\left(H_w f_w + H_g^s f_g\right)\right) = \\ = \Lambda\frac{dQ}{d\xi} + \frac{d}{d\xi}\left(\left(H_w - H_g^s\right)\Omega\frac{dS_w}{d\xi}\right) + \frac{d}{d\xi}\left(\kappa\frac{dT}{d\xi}\right), \end{aligned} \tag{A.4}$$

$$\frac{dQ}{d\xi} = q. \tag{A.5}$$

We integrate Eqs. (A.2) – (A.4) once and use that $\frac{dS_w}{d\xi} \to 0$, $Q \to 0$ and $\frac{dT}{d\xi} \to 0$ for $\xi \to -\infty$, in such a way that $S_w \to S_w^-$ and $T \to T^-$, obtaining

$$\rho_w \Omega \frac{dS_w}{d\xi} = (-Q - \varphi v^{SCF}\rho_w S_w + \rho_w u f_w) - (-\varphi v^{SCF}\rho_w^- S_w^- + \rho_w^- u^- f_w^-), \tag{A.6}$$

$$\rho_g \Omega \frac{dS_w}{d\xi} = (-Q + \varphi v^{SCF}\rho_g S_g - \rho_g u f_g) - (\varphi v^{SCF}\rho_g^- S_g^- - \rho_g^- u^- f_g^-), \tag{A.7}$$

$$\begin{aligned} (H_w - H_g^s)\Omega\frac{dS_w}{d\xi} + \kappa\frac{dT}{d\xi} &= -v^{SCF}(H_r + \varphi H_w S_w + \varphi H_g^s S_g) + u(H_w f_w + H_g^s f_g) - \Lambda Q \\ &\quad + v^{SCF}(H_r^- + \varphi H_w^- S_w^- + \varphi H_g^{s-} S_g^-) - u^-(H_w^- f_w^- + H_g^{s-} f_g^-), \end{aligned} \tag{A.8}$$

$$\frac{dQ}{d\xi} = q. \tag{A.9}$$

Remark 15. *By letting ξ tend to $+\infty$ in Eq.* (A.6), *we recover the Rankine–Hugoniot condition:*

$$Q^+ = u^+\rho_w^+ f_w^+ - u^-\rho_w^- f_w^- - \varphi v^{SCF}(\rho_w^+ S_w^+ - \rho_w^- S_w^-), \tag{A.10}$$

and since $S_g^+ = 0$, it follows from Eq. (A.7) *that*

$$Q^+ = \rho_g^- \left(u^- f_g^- - \varphi v^{SCF} S_g^-\right). \tag{A.11}$$

A similar limiting procedure in Eq. (A.8) *recovers the other Rankine–Hugoniot condition:*

$$\begin{aligned}\Lambda Q^+ &= u^+(H_w^+ f_w^+ + H_g^{s+} f_g^+) - u^-(H_w^- f_w^- + H_g^{s-} f_g^-)\\ &-v^{SCF}\Big[(H_r^+ + \varphi H_w^+ S_w^+ + \varphi H_g^{s+} S_g^+) - (H_r^- + \varphi H_w^- S_w^- + \varphi H_g^{s-} S_g^-)\Big].\end{aligned} \tag{A.12}$$

We can divide the equations (A.6), (A.7) by the densities, and obtain

$$\Omega \frac{dS_w}{d\xi} = \left(-\frac{Q}{\rho_w} - \varphi v^{SCF} S_w + u f_w\right) - \frac{\rho_w^-}{\rho_w}\left(-\varphi v^{SCF} S_w^- + u^- f_w^-\right), \tag{A.13}$$

$$\Omega \frac{dS_w}{d\xi} = \left(-\frac{Q}{\rho_g} + \varphi v^{SCF} S_g - u f_g\right) - \frac{\rho_g^-}{\rho_g}\left(\varphi v^{SCF} S_g^- - u^- f_g^-\right). \tag{A.14}$$

Subtracting Eq. (A.14) from Eq. (A.13) we obtain $u = u(Q,T)$ as

$$u = Q\left(\frac{1}{\rho_w} - \frac{1}{\rho_g}\right) + \varphi v^{SCF} + \frac{\rho_w^-}{\rho_w}\left(-\varphi v^{SCF} S_w^- + u^- f_w^-\right) + \frac{\rho_g^-}{\rho_g}\left(-\varphi v^{SCF} S_g^- + u^- f_g^-\right). \tag{A.15}$$

Remark 16. *Letting $\xi \to +\infty$ in Eq.* (A.15), *we obtain $u^+ =$*

$$Q^+\left(\frac{1}{\rho_w^+} - \frac{1}{\rho_g^+}\right) + \varphi v^{SCF} + \left(\frac{\rho_w^-}{\rho_w^+} - \frac{\rho_g^-}{\rho_g^+}\right)\left(u^- f_w^- - \varphi v^{SCF} S_w^-\right) + \frac{\rho_g^-}{\rho_g^+}\left(u^- - \varphi v^{SCF}\right). \tag{A.16}$$

This equation can also be obtained from Eqs. (A.10) *and* (A.11)

Multiplying Eq. (A.13) by H_w, Eq. (A.14) by H_g^s and subtracting we obtain

$$\begin{aligned}\left(H_w - H_g^s\right)\Omega\frac{dS_w}{d\xi} &= -Q\left(\frac{H_w}{\rho_w} - \frac{H_g^s}{\rho_g}\right) - \varphi v^{SCF}\left(H_w S_w + H_g^s S_g\right)\\ &+ u\left(H_w f_w + H_g^s f_g\right) - \frac{\rho_w^-}{\rho_w} H_w\left(-\varphi v^{SCF} S_w^- + u^- f_w^-\right) + \frac{\rho_g^-}{\rho_g} H_g^s\left(\varphi v^{SCF} S_g^- - u^- f_g^-\right).\end{aligned} \tag{A.17}$$

Subtracting this equation from Eq. (A.8) we obtain

$$\begin{aligned}\kappa\frac{\partial T}{\partial \xi} &= Q\left(\frac{H_w}{\rho_w} - \frac{H_g^s}{\rho_g} - \Lambda\right) - \varphi v^{SCF}\left(\rho_w^-\left(\frac{H_w}{\rho_w} - \frac{H_w^-}{\rho_w^-}\right)S_w^- + \rho_g^-\left(\frac{H_g^s}{\rho_g} - \frac{H_g^{s-}}{\rho_g^-}\right)S_g^-\right)\\ &-v^{SCF}(H_r - H_r^-) + u^-\left(\rho_w^-\left(\frac{H_w}{\rho_w} - \frac{H_w^-}{\rho_w^-}\right)f_w^- + \rho_g^-\left(\frac{H_g^s}{\rho_g} - \frac{H_g^{s-}}{\rho_g^-}\right)f_g^-\right).\end{aligned} \tag{A.18}$$

The enthalpies used above are only functions of temperature. Note that the ratios of the enthalpies per unit volume and the densities can be interpreted as enthalpies per unit mass. Thus, it is useful to define enthalpies per unit mass $h_w(T)$, $h_r(T)$, $h_g(T)$ ($[J/kg]$) as enthalpies per unit volume H_r, H_w, H_g ($[J/m^3]$) divided by the respective densities at the temperature of interest.

Subtracting Eq. (A.6) from Eq. (A.7) we obtain

$$(\rho_w - \rho_g)\Omega\frac{dS_w}{d\xi} = -\varphi v^{SCF}(\rho_w S_w + \rho_g S_g) + u(\rho_w f_w + \rho_g f_g) + \varphi v^{SCF}(\rho_w^- S_w^- + \rho_g^- S_g^-) - u^-(\rho_w^- f_w^- + \rho_g^- f_g^-). \tag{A.19}$$

If we divide the RHS of Eq. (A.19) by ρ_w, and choose v^{SCF} as given by Eq. (2.33), we see that (S_w, S_g, u) given by (S_w^-, S_g^-, u^-) and $(S_w^+ = 1, S_g^+ = 0, u^+)$ where $u^+ = u^0$ is given by Eq. (2.32), $S_w^+ < S_w^*$, $S_g^+ = 1 - S_w^+$ are equilibria for the ordinary differential equation (A.19).

For an orbit to exist between the equilibria $(-)$ and $(+)$, it is necessary and sufficient that there is no other equilibrium in between, yielding Oleĭnik's construction.

Appendix B. General linear analysis at equilibria

To plot conveniently, the independent variables will be reordered as Q, T, S_w. We have to analyze the following ODE's, with fluxes given by F^Q, $\kappa^{-1}F^T$, and $\Omega^{-1}F^w$ defined below. From Eqs. (A.9) and (1.13):

$$\frac{dQ}{d\xi} = q_b\,(S_w - 1)\left(T - T^b\right) := F^Q \tag{B.1}$$

From Eq. (A.18), dividing by κ:

$$\frac{\partial T}{\partial \xi} = \kappa^{-1}\Bigg(Q\Big(\frac{H_w}{\rho_w} - \frac{H_g^s}{\rho_g} - \Lambda\Big) - v^{SCF}(H_r - H_r^-) - \varphi v^{SCF}\Bigg(S_w^-\rho_w^-\Big(\frac{H_w}{\rho_w} - \frac{H_w^-}{\rho_w^-}\Big) + S_g^-\rho_g^-\Big(\frac{H_g^s}{\rho_g} - \frac{H_g^{s-}}{\rho_g^-}\Big)\Bigg) + u^-\Bigg(f_w^-\rho_w^-\Big(\frac{H_w}{\rho_w} - \frac{H_w^-}{\rho_w^-}\Big) + f_g^-\rho_g^-\Big(\frac{H_g^s}{\rho_g} - \frac{H_g^{s-}}{\rho_g^-}\Big)\Bigg)\Bigg) := \kappa^{-1}F^T. \tag{B.2}$$

From Eq. (A.19), dividing by $(\rho_w - \rho_g)\,\Omega$:

$$\frac{dS_w}{d\xi} = \Omega^{-1}\Bigg(-\varphi v^{SCF}\frac{\rho_g}{\rho_w - \rho_g} + u\frac{\rho_g}{\rho_w - \rho_g} + uf_w + \varphi v^{SCF}S_w^-\frac{\rho_w^- - \rho_g^-}{\rho_w - \rho_g} - \varphi v^{SCF}S_w + \varphi v^{SCF}\frac{\rho_g^-}{\rho_w - \rho_g} - u^-\frac{\rho_g^-}{\rho_w - \rho_g} - u^- f_w^-\frac{\rho_w^- - \rho_g^-}{\rho_w - \rho_g}\Bigg) := \Omega^{-1}F^w. \tag{B.3}$$

Notice that the right hand side of Eq. (B.3) depends on the S_w, T and Q, while the right hand side of Eq. (B.2) depends on the T and Q, and the right hand side of Eq. (B.1) depends on the S_w and T.

When we evaluate Eq. (A.15) at state $(-)$, we obtain the following expression for the total velocity u:

$$u = \frac{\rho_w^-}{\rho_w}u^- + Q\left(\frac{1}{\rho_w} - \frac{1}{\rho_g}\right) + \varphi v^{SCF}\left(1 - \frac{\rho_w^-}{\rho_w}\right) + \left(\frac{\rho_g^-}{\rho_g} - \frac{\rho_w^-}{\rho_w}\right)F^-, \tag{B.4}$$

with $F^- = u^- f_g^- - \varphi v^{SCF} S_g^-$.

Remark 17. *Equation* (B.4) *states that there are two reasons why* u *changes across a steam condensation front. The first reason is that* ρ_g *and* ρ_w *change with temperature, so that the last two terms on the RHS of Eq.* (B.4) *contribute to changing* u*. However, there is a* *second reason, which is important even if the densities do not change with temperature. The first term on the RHS of Eq.* (B.4) *is proportional to the total amount of heat released Q. Therefore, this term contributes to changing u, unless at special situations when the water and steam density are equal, i.e. at the critical point.*

B.1. **The Jacobian at a generic equilibrium.** From Eq. (B.4), we obtain

$$\frac{\partial u}{\partial Q} = \left(\frac{1}{\rho_w} - \frac{1}{\rho_g}\right), \tag{B.5}$$

$$\frac{\partial u}{\partial T} = Q\left(\frac{\alpha_w}{\rho_w} - \frac{\alpha_g}{\rho_g}\right) - \varphi v^{SCF}\frac{\alpha_w \rho_w^-}{\rho_w} + \left(\frac{\alpha_g \rho_g^-}{\rho_g} - \frac{\alpha_w \rho_w^-}{\rho_w}\right) F^-, \tag{B.6}$$

$$\frac{\partial u}{\partial S_w} = 0. \tag{B.7}$$

We have used in Eq. (B.6) that $\partial(\rho^{-1})/\partial T = -\rho^{-2}\,\partial\rho/\partial T = \alpha/\rho$.

Now we turn to find the general Jacobian matrix. From the RHS of Eq. (B.1):

$$F^Q = q_b\left(S_w - 1\right)\left(T - T^b\right), \tag{B.8}$$

$$\frac{\partial F^Q}{\partial Q} = 0, \tag{B.9}$$

$$\frac{\partial F^Q}{\partial T} = q_b\left(S_w - 1\right), \tag{B.10}$$

$$\frac{\partial F^Q}{\partial S_w} = q_b\left(T - T^b\right). \tag{B.11}$$

We rewrite the RHS of Eq. (B.2) as

$$\begin{aligned} F^T = \Bigg(& Q(h_w - h_g^s - \Lambda) - v^{SCF}(H_r - H_r^-) - \varphi v^{SCF}\Bigg(S_w^- \rho_w^-(h_w - h_w^-) \\ & + S_g^- \rho_g^-(h_g^s - h_g^{s-})\Bigg) + u^-\left(f_w^- \rho_w^-(h_w - h_w^-) + f_g^- \rho_g^-(h_g^s - h_g^{s-})\right)\Bigg), \end{aligned} \tag{B.12}$$

$$J_{21} = \frac{\partial}{\partial Q}(\kappa^{-1}F^T) = \kappa^{-1}\left(h_w - h_g^s - \Lambda\right), \tag{B.13}$$

$$\begin{aligned} J_{22} = \frac{\partial}{\partial T}(\kappa^{-1}F^T) = \kappa^{-1}\Bigg(& Q(c_w^p - c_g^p) - v^{SCF}C_r^p \\ & - \varphi v^{SCF}\left(S_w^- \rho_w^- c_w^{p-} + S_g^- \rho_g^- c_g^{p-}\right) + u^-(f_w^- \rho_w^- c_w^{p-} + f_g^- \rho_g^- c_g^{p-})\Bigg), \end{aligned} \tag{B.14}$$

$$J_{23} = \frac{\partial}{\partial S_w}(\kappa^{-1}F^T) = \frac{\varphi(\kappa_w - \kappa_g)}{\kappa}F^T. \tag{B.15}$$

From the RHS of Eq. (B.3), we obtain, for

$$J_{31} = \frac{\partial}{\partial Q}(\Omega^{-1}F^w), \quad J_{21} = \frac{\partial}{\partial T}(\Omega^{-1}F^w), \quad J_{11} = \frac{\partial}{\partial S_w}(\Omega^{-1}F^w),$$

$$J_{31} = \Omega^{-1}\left(f_w + \frac{\rho_g}{\rho_w - \rho_g}\right)\left(\frac{1}{\rho_w} - \frac{1}{\rho_g}\right),$$

$$J_{21} = \Omega^{-1}\left((u - \varphi v^{SCF})\Xi_3 - (u^- f_w^- - \varphi v^{SCF} S_w^-)\Xi_1 - (u^- - \varphi v^{SCF})\Xi_2) - \Omega^{-1}\frac{\partial\Omega}{\partial T}F^w\right),$$

$$J_{11} = \Omega^{-1}\left(-\varphi v^{SCF} + u\frac{\partial f_w}{\partial S_w}\right) - \Omega^{-2}\frac{\partial\Omega}{\partial S_w}F^w, \tag{B.16}$$

where

$$\Xi_1 = \frac{\rho_w^- - \rho_g^-}{(\rho_w - \rho_g)^2}(\rho_w\alpha_w - \rho_g\alpha_g), \qquad \Xi_2 = \frac{\rho_g^-}{(\rho_w - \rho_g)^2}(\rho_w\alpha_w - \rho_g\alpha_g), \tag{B.17}$$

$$\Xi_3 = \frac{\rho_g}{(\rho_w - \rho_g)^2}(\rho_w\alpha_w - \rho_g\alpha_g) + \Xi_4, \quad \text{and} \quad \Xi_4 = -\frac{\rho_g\alpha_g}{\rho_w - \rho_g}. \tag{B.18}$$

Thus, the Jacobian of the System (B.1)–(B.3) at any equilibrium point is

$$\mathbf{J} = \begin{pmatrix} 0 & q_b\,(S_w - 1) & q_b\left(T - T^b\right) \\ J_{21} & J_{22} & 0 \\ J_{31} & J_{32} & J_{33} \end{pmatrix}. \tag{B.19}$$

B.2. **The left equilibria.** Let us search for left equilibria. On the left side of the SCF, at left equilibria $(-)$ the temperature is the boiling temperature from the physics, *i.e.*, $T = T^b$ and $Q = 0$ from Eq. (A.1), so that F^Q and F^T in Eqs. (B.1) and (B.2) vanish. Similarly, from Eq. (B.4) we see that $u = u^-$. Thus, the RHS of Eq. (B.3) becomes

$$\Omega^{-1}F^w = \varphi v^{SCF}(S_w^- - S_w) - u^-\left(f_w(S_w^-, T^b) - f_w(S_w, T^b)\right). \tag{B.20}$$

Therefore, $\Omega^{-1}F^w$ vanishes for $S_w^- = S_w$. This shows that one left equilibrium is $(Q, T, S_w) = (0, T^b, S_w^-)$.

Notice that $\Omega^{-1}F^w$ in Eq. (B.20) vanishes if and only if

$$f_w(S_w, T^b) - f_w^-(S_w, T^b) - \frac{\varphi v^{SCF}}{u^-}(S_w - S_w^-) = 0. \tag{B.21}$$

This equation is identical to the Rankine–Hugoniot condition from the saturation S_w^- to S_w for the fractional flow of water at temperature T^b, for a discontinuity with speed $(\varphi v^{SCF})/u^-$. There is always one solution S_w^-. Depending on the value of the speed (which we cannot discuss without taking into account the right equilibrium of the SCF orbit), there may be no other solution, one, two, or a double solution for Eq. (B.21). We will return to this matter in Section F on the phase portrait.

B.2.1. *The Jacobian at the (minus) upstream side.* At the upstream side equilibrium where $(Q, T_w, S_w) = (0, T^b, S_w^-)$, we use Eq. (B.19) and obtain:

$$\mathbf{J}^- = \begin{pmatrix} 0 & -q_b\,(1 - S_w^-) & 0 \\ -\frac{1}{\kappa^-}\Lambda(T^-) & J_{22} & 0 \\ J_{31}^- & J_{32}^- & J_{33}^- \end{pmatrix} \tag{B.22}$$

where

$$J_{33}^{-} = \frac{1}{\Omega^{-}}\left(-\varphi v^{SCF} + u\frac{\partial f_w}{\partial S_w}\right)^{-} \tag{B.23}$$

and

$$J_{32}^{-} = \frac{1}{\Omega^{-}}\Big(\left(u^{-} - \varphi v^{SCF}\right)\Xi_4^{-} - \left(u^{-} f_w^{-} - \varphi v^{SCF} S_w^{-}\right)\Xi_1^{-}\Big). \tag{B.24}$$

We notice that

$$\Xi_4^{-} = \left(\Xi_3^{-} - \Xi_2^{-}\right) = -\frac{\rho_g^{-}\alpha_g^{-}}{\rho_w^{-} - \rho_g^{-}}.$$

and use that

$$\Lambda(T^{-}) = \Lambda(T^{0}) - h_w^{-} + h_g^{s-}. \tag{B.25}$$

B.2.2. *Eigenvalues and eigenvectors at the (minus) upstream side.* We can calculate the eigenvalues at the (minus) upstream side.

We abbreviate the matrix $\mathbf{J}^{-}$ in Eq. (B.22) and define D as

$$\mathbf{J}^{-} = \begin{pmatrix} 0 & -F & 0 \\ -E & -G & 0 \\ -C & b & -A \end{pmatrix}, \qquad D = G + \sqrt{G^2 + 4EF}. \tag{B.26}$$

For $\mathbf{J}^{-}$ the eigenvalues $\mu_{(+)}^{-}$, $\mu_{(-)}^{-}$, and $\mu_{(s)}^{-}$ and corresponding eigenvectors are:

$$\mu_{(+)}^{-} = \frac{2EF}{D},\ \mu_{(-)}^{-} = -\frac{D}{2}, \text{ with eigenvectors: } \begin{pmatrix} -\frac{2EF+AD}{2bE+CD} \\ \frac{2E}{D}\frac{2EF+AD}{2bE+CD} \\ 1 \end{pmatrix}, \begin{pmatrix} -\frac{D-2A}{bD-2CF}F \\ -\frac{D}{2}\frac{D-2A}{bD-2CF} \\ 1 \end{pmatrix}; \tag{B.27}$$

$$\mu_{(s)}^{-} = -A \qquad \text{with eigenvector: } \begin{pmatrix} 0 \\ 0 \\ 1 \end{pmatrix}. \tag{B.28}$$

We observe that $\mu_{(-)}^{-} < 0 < \mu_{(+)}^{-}$. From information upstream of the SCF we know that $\mu_{(s)}^{-} \leqq 0$. (Only for high quality steam injection.)

B.3. **The right equilibrium.** At the (+) side, the physics dictates that $S_w = 1$ (temperature yet unspecified), so that the RHS of Eq. (B.1) vanishes, namely $\digamma^{Q} = 0$. Using $S_w = 1$, $u = u^{+}$ on the RHS of Eq. (B.3), or better, (A.19), we see that at a (+) equilibrium:

$$(\rho_w^{+} - \rho_g^{+})\digamma^{w} = \varphi v^{SCF}(\rho_w^{-}S_w^{-} + \rho_g^{-}S_g^{-} - \rho_w^{+}) - u^{-}(\rho_w^{-}f_w^{-} + \rho_g^{-}f_g^{-}) + u^{+}\rho_w^{+}.$$

From Eq. (B.4), the velocity u at any point can be expressed as Eq. (A.15) in the dependent variable ξ. Also, the velocity at the downstream side is given by Eq. (A.16) or (2.32):

We claim that there is a single downstream equilibrium. First of all $\digamma^{Q}$ certainly vanishes at $S_w = 1$. Moreover $\digamma^{w}$ vanishes at the edge $Q = Q^{+}$ and $S_w = 1$ (see Lemma F.1). Finally $\digamma^{T}$ vanishes at the edge $Q = Q^{+}$ and $T = T^{0}$.

B.3.1. *The Jacobians at the (plus) downstream side.*

$$J_{33}^{+} = \frac{1}{\Omega^{+}}\left(-\varphi v^{SCF} + u^{+}\frac{\partial f_w^{+}}{\partial S_w^{+}}\right) + \frac{1}{\Omega^{+}}\frac{\partial \Omega}{\partial S_w}\left(\mathcal{F}^{w}\right)^{+} = -\frac{1}{\Omega^{+}}\varphi v^{SCF} < 0,$$
$$J_{32}^{+} = 0 \quad \text{(for the proof see Section B.3.2)},$$
$$J_{31}^{+} = \frac{1}{\Omega^{+}}\left(1 + \frac{\rho_g}{\rho_w - \rho_g}\right)^{+}\left(\frac{1}{\rho_w} - \frac{1}{\rho_g}\right)^{+} = -\frac{1}{\Omega^{+}}\frac{1}{\rho_g^{+}} < 0,$$
$$J_{21}^{+} = 0.$$

This is so because neither $\mathcal{F}^{T}$ nor the RHS of Eqs. (A.18) or (B.2) contain the saturations and because $\mathcal{F}^{T}$ is zero both at the upstream and downstream sides.

$$J_{22}^{+} = \frac{1}{\kappa^{+}}\Big(Q^{+}(c_w^{p+} - c_g^{p+}) - v^{SCF}C_r^{p} - \varphi v^{SCF}(S_w^{-}\rho_w^{-}c_w^{p+} + S_g^{-}\rho_g^{-}c_g^{p+})$$
$$+u^{-}(f_w^{-}\rho_w^{-}c_w^{p+} + f_g^{-}\rho_g^{-}c_g^{p+})\Big),$$

where c_w^p and c_g^p denote the temperature derivative of h_w and h_g^s.

Calculations show that J_{22}^{+} is negative, and

$$J_{21}^{+} = \frac{1}{\kappa^{+}}(h_w - h_g^s - \Lambda)^{+} = -\frac{1}{\kappa^{+}}\Lambda\left(T^{0}\right) < 0, \tag{B.29}$$
$$J_{13}^{+} = -q_b\left(T^{b} - T\right)^{+} = -q_b\left(T^{b} - T^{0}\right) < 0, \tag{B.30}$$
$$J_{12}^{+} = -q_b\left(1 - S_w\right)^{+} = 0, \tag{B.31}$$
$$J_{11}^{+} = 0. \tag{B.32}$$

B.3.2. *Proof that $J_{32}^{+} = 0$.* From Eq. (B.20), the derivative of the velocity versus temperature evaluated at the downstream side is:

$$\frac{\partial u^{+}}{\partial T} = Q^{+}\left(\frac{\alpha_w^{+}}{\rho_w^{+}} - \frac{\alpha_g^{+}}{\rho_g^{+}}\right) + \left(\frac{\alpha_w^{+}\rho_w^{-}}{\rho_w^{+}} - \frac{\alpha_g^{+}\rho_g^{-}}{\rho_g^{+}}\right)\left(u^{-}f_w^{-} - \varphi v^{SCF}S_w^{-}\right) + \frac{\alpha_g^{+}\rho_g^{-}}{\rho_g^{+}}\left(u^{-} - \varphi v^{SCF}\right).$$

Let us examine the RHS of Eq. (A.19). Notice that the right hand side of this equation is zero when evaluated both at the upstream and the downstream side. As our purpose is to prove that the derivative versus temperature of the right hand side (part of the Jacobian J_{32}^{+}) is zero, we only need to prove that the derivative versus temperature of the right hand side is zero. Hence the Jacobian evaluated at the downstream side J_{32}^{+} can be written as

$$J_{32}^{+}\left(\rho_w^{+} - \rho_g^{+}\right)\Omega^{+} = \varphi v^{SCF}\rho_w^{+}\alpha_w^{+} - u^{+}\rho_w^{+}\alpha_w^{+} + \frac{\partial u^{+}}{\partial T^{+}}\rho_w^{+},$$

where we use that at the downstream side $S_w = 1$ and $S_g = 0$. Moreover we defined the thermal expansion coefficient at constant pressure of water and steam respectively as

$$\alpha_w = -\frac{1}{\rho_w}\left(\frac{\partial \rho_w}{\partial T}\right)_p, \qquad \alpha_g = -\frac{1}{\rho_g}\left(\frac{\partial \rho_g}{\partial T}\right)_p. \tag{B.33}$$

We continue to substitute the temperature derivative of the velocity versus temperature and the downstream velocity given above

$$
\begin{aligned}
&J_{32}^{+}\left(\rho_w^{+}-\rho_g^{+}\right)\Omega^{+}=\varphi v^{SCF}\rho_w^{+}\alpha_w^{+}-\\
&\rho_w^{+}\alpha_w^{+}\left(Q^{+}\big(\frac{1}{\rho_w^{+}}-\frac{1}{\rho_g^{+}}\big)+\varphi v^{SCF}+\big(\frac{\rho_w^{-}}{\rho_w^{+}}-\frac{\rho_g^{-}}{\rho_g^{+}}\big)(u^{-}f_w^{-}-\varphi v^{SCF}S_w^{-})+\frac{\rho_g^{-}}{\rho_g^{+}}(u^{-}-\varphi v^{SCF})\right)\\
&+\rho_w^{+}\left(Q^{+}\big(\frac{\alpha_w^{+}}{\rho_w^{+}}-\frac{\alpha_g^{+}}{\rho_g^{+}}\big)+\big(\frac{\alpha_w^{+}\rho_w^{-}}{\rho_w^{+}}-\frac{\alpha_g^{+}\rho_g^{-}}{\rho_g^{+}}\big)(u^{-}f_w^{-}-\varphi v^{SCF}S_w^{-})+\frac{\alpha_g^{+}\rho_g^{-}}{\rho_g^{+}}(u^{-}-\varphi v^{SCF})\right).
\end{aligned}
$$

We carry out the multiplication and simplify:

$$
\begin{aligned}
J_{32}^{+}\left(\rho_w^{+}-\rho_g^{+}\right)\Omega^{+}=\varphi v^{SCF}(\rho_w^{+}\alpha_w^{+})-\Bigg(&Q^{+}\big(\alpha_w^{+}-\frac{\rho_w^{+}\alpha_w^{+}}{\rho_g^{+}}\big)+\rho_w^{+}\alpha_w^{+}\varphi v^{SCF}\\
&+\big(\rho_w^{-}\alpha_w^{+}-\frac{\rho_g^{-}\rho_w^{+}\alpha_w^{+}}{\rho_g^{+}}\big)(u^{-}f_w^{-}-\varphi v^{SCF}S_w^{-})+\frac{\rho_g^{-}\rho_w^{+}\alpha_w^{+}}{\rho_g^{+}}(u^{-}-\varphi v^{SCF})\Bigg)\\
+\Bigg(Q^{+}\big(\alpha_w^{+}-\frac{\alpha_g^{+}\rho_w^{+}}{\rho_g^{+}}\big)+\big(\alpha_w^{+}\rho_w^{-}-\frac{\alpha_g^{+}\rho_g^{-}\rho_w^{+}}{\rho_g^{+}}\big)&(u^{-}f_w^{-}-\varphi v^{SCF}S_w^{-})+\frac{\alpha_g^{+}\rho_g^{-}\rho_w^{+}}{\rho_g^{+}}(u^{-}-\varphi v^{SCF})\Bigg).
\end{aligned}
\tag{B.34}
$$

We observe that a number of the above terms cancel:

$$
\begin{aligned}
J_{32}^{+}\left(\rho_w^{+}-\rho_g^{+}\right)\Omega^{+}=&\Big(Q^{+}\frac{\rho_w^{+}\alpha_w^{+}}{\rho_g^{+}}+\frac{\rho_g^{-}\rho_w^{+}\alpha_w^{+}}{\rho_g^{+}}\left(u^{-}f_w^{-}-\varphi v^{SCF}S_w^{-}\right)-\frac{\rho_g^{-}\rho_w^{+}\alpha_w^{+}}{\rho_g^{+}}\left(u^{-}-\varphi v^{SCF}\right)\Big)\\
&+\Big(-Q^{+}\frac{\alpha_g^{+}\rho_w^{+}}{\rho_g^{+}}-\frac{\alpha_g^{+}\rho_g^{-}\rho_w^{+}}{\rho_g^{+}}\left(u^{-}f_w^{-}-\varphi v^{SCF}S_w^{-}\right)+\frac{\alpha_g^{+}\rho_g^{-}\rho_w^{+}}{\rho_g^{+}}\left(u^{-}-\varphi v^{SCF}\right)\Big).
\end{aligned}
\tag{B.35}
$$

Now we use that $(u^{-}-\varphi v^{SCF})-(u^{-}f_w^{-}-\varphi v^{SCF}S_w^{-})=(u^{-}f_g^{-}-\varphi v^{SCF}S_g^{-})$ and we obtain:

$$
\begin{aligned}
J_{32}^{+}\left(\rho_w^{+}-\rho_g^{+}\right)\Omega^{+}=&\frac{\rho_w^{+}\alpha_w^{+}}{\rho_g^{+}}Q^{+}-\frac{\rho_g^{-}\rho_w^{+}\alpha_w^{+}}{\rho_g^{+}}\left(u^{-}f_g^{-}-\varphi v^{SCF}S_g^{-}\right)\\
&-\frac{\rho_w^{+}\alpha_g^{+}}{\rho_g^{+}}Q^{+}+\frac{\alpha_g^{+}\rho_g^{-}\rho_w^{+}}{\rho_g^{+}}\left(u^{-}f_g^{-}-\varphi v^{SCF}S_g^{-}\right).
\end{aligned}
$$

As we have that

$$
Q^{+}=\rho_g^{-}\left(u^{-}f_g^{-}-\varphi v^{SCF}S_g^{-}\right),
$$

so we immediately observe that

$$
J_{32}^{+}\left(\rho_w^{+}-\rho_g^{+}\right)\Omega^{+}=0.
$$

B.3.3. *Eigenvalues and eigenvectors at the (plus) downstream side.* (For the equilibrium with $T = T^0$.)

The Jacobian matrix has the form

$$\mathbf{J}^+ = \begin{pmatrix} 0 & 0 & -q_b(T^b - T^+) \\ -\frac{1}{\kappa^+}\Lambda\,(T^0) & J_{22}^+ & 0 \\ -\frac{1}{\Omega^+}\frac{1}{\rho_g^+} & 0 & -\frac{1}{\Omega^+}\varphi v^{SCF} \end{pmatrix}; \tag{B.36}$$

we abbreviate it and define D as follows

$$\mathbf{J}^+ = \begin{pmatrix} 0 & 0 & -F \\ -E & -C & 0 \\ -B & 0 & -A \end{pmatrix}, \qquad D = A + \sqrt{(A^2 + 4FB)}. \tag{B.37}$$

We use Maple to find the following eigenvectors and eigenvalues.

For the positive eigenvalue we find $\mu_{(+)}^+$, with eigenvector:

$$\mu_{(+)}^+ = -\frac{1}{2}A + \frac{1}{2}\sqrt{(A^2 + 4FB)} = \frac{2FB}{D} > 0, \qquad \begin{pmatrix} \frac{-2FB-CD}{ED} \\ 1 \\ \frac{2B}{D}\frac{2FB+CD}{ED} \end{pmatrix}. \tag{B.38}$$

One of the negative eigenvalues is $\mu_{(T)}^+$,

$$\mu_{(T)}^+ = -C, \qquad \text{with eigenvector:} \qquad \begin{pmatrix} 0 \\ 1 \\ 0 \end{pmatrix}; \tag{B.39}$$

and finally we have the other negative eigenvalue $\mu_{(T)}^+$,

$$\mu_{(T)}^+ = -\frac{1}{2}D, \qquad \text{with eigenvector:} \qquad \begin{pmatrix} \frac{D+2C}{2E} \\ 1 \\ \frac{D(D-2C)}{4EF} \end{pmatrix}. \tag{B.40}$$

Appendix C. Steam condensation travelling wave under the injection of high quality steam

We will study the situation where the SCF speed is chosen to satisfy the steam-water bifurcation condition. This is the SCF arising in Riemann problems of type I. Otherwise, there would be two left equilibria and one right equilibrium. This is the case when the steam injection has high quality, *i.e.* it is either pure $S_g^{inj} = 1$ or at least $1 - S_\dagger < S_g^{inj}$. Then the Riemann solution has structure I. (The case when $1 - S_* < S_g^{inj} < 1 - S_\dagger$, which would give rise to a Riemann solution with structure II, has yet to be analyzed.)

For pure steam, it is easy to see that there are only two equilibrium points in the physical space. By physical space we mean the space spanned by $0 \leq Q < Q^+$, $T^0 \leq T < T^b$, $S_{wc} \leq S_w < 1$.

To avoid the mathematical complication due to the fact that Ω defined in Equation (1.10) and used in equations (A.2), (A.3) and (A.4) vanishes at the equilibria, we will use a constant representative value in our numerical computations viz. $6 \times 10^{-5}[m^2/s]$. For simplicity we also use a constant value for the thermal conductivity $\kappa(s_w = 0.5) = \kappa_r + 0.5\varphi\kappa_w + 0.5\varphi\kappa_g$

C.1. **Local analysis of the right (downstream=(+)) state.** We consider the reservoir being initially saturated with water $S_w = 1.0$. The reservoir temperature is 293 K. The cumulative condensation rate Q^+ is given by the expression

$$Q^+ = \rho_g^-(u^- f_g^- - \varphi v^{SCF} S_g^-)$$

where $v^{SCF} = 7.3840124530689 \times 10^{-6}\,\mathrm{m/s}$ is the velocity of the steam condensation front obtained under the condition that the rarefaction wave velocity in the steam zone equals v^{SCF}. The steam saturation $S_g^- = 0.69195796010529$ is obtained in the same way.

Thus the right equilibrium (+) for the ODE is

$$\left(Q^+, T^+, S_w^+\right) = \left(0.55893328137576 \times 10^{-3}, 293, 1\right)$$

In evaluating the Jacobians we use constant values for the capillary diffusion coefficient $\Omega = 0.00006[m^2/s]$ and we also use a saturation independent thermal conductivity $\kappa = 1.957832[W/(mK)]$ *i.e.*, the thermal conductivity evaluated at $S_w = 0.5$. The Jacobian at the plus side is as follows

$$J^+ = \begin{pmatrix} 0 & 0 & -0.80149999999991 \\ -1.2554671173798 \times 10^{-6} & -8.0231129093879 & 0 \\ -2.2261371170696 \times 10^{-4} & 0 & -0.046759616048425 \end{pmatrix} \quad \text{(C.1)}$$

There is one positive eigenvalue $y_1 = 133.55$. The negative eigenvalues are the weak eigenvalue $y_2 = -8.0231129093879$ and the strong eigenvalue $y_3 = -133.59920353079$ with eigenvectors

$$\mathbf{v}_2 = \begin{pmatrix} 0 \\ 1 \\ 0 \end{pmatrix} \quad \text{and} \quad \mathbf{v}_3 = \begin{pmatrix} 0.11280448088178 \times 10^{-3} \\ 1 \\ 0.016672547318581 \end{pmatrix} \quad \text{(C.2)}$$

respectively.

Therefore the stable manifold $W^s(+)$ (along which the orbits are attracted to (+)) is two dimensional. It contains the point (+) and it is tangent at that point to the vectors $\mathbf{v}_2$ and $\mathbf{v}_3$. It is not hard to verify $dQ/d\xi = 0$ is zero along the line $S_w = 1$ and $Q = Q^+$. It is also possible to show that $dS_w/d\xi = 0$ along the line $S_w = 1$ and $Q = Q^+$. An orbit for the full system is tangent to this line. Because it corresponds to the weakest eigenvalue all orbits in $W^s(+)$ within physical space are attracted to it. If any orbit arrives at the (+) equilibrium at the opposite side of the strong orbit tangent to $\mathbf{v}_3$, it is physically unacceptable as it arrives from the outside of the physical space. We conclude that if a connection between $W^u(-)$ and $W^s(+)$ exists arriving through the strong eigenvector a bifurcation occurs. The picture is summarized in Figure F.1. Note that we have not drawn the Figure to scale but to enhance its illustrative purpose.

C.2. **Local analysis of the left (upstream=(-)) state.** We consider the injection conditions where we inject pure steam at the normal boiling point of water $T^b = 373.15$. A rarefaction wave follows and at the upstream side we use the condition that the rarefaction wave velocity in the steam zone equals v^{SCF}. Consequently the water saturation at the upstream side is $S_w^- = 0.30804203989471$. The cumulative condensation is still zero.

Thus the left equilibrium $(-)$ for the ODE is

$$\left(Q^-, T^-, S_w^-\right) = (0, 373.15, 0.30804203989471)$$

The Jacobian at the $(-)$ equilibrium is as follows

$$J^- = \begin{pmatrix} 0 & -0.0069195796010545 & 0 \\ -1.1516024651448 \times 10^6 & -8.7389251829442 & 0 \\ -20.330947447114 & 3.6720211572508 \times 10^{-5} & 0 \end{pmatrix} \tag{C.3}$$

There is one negative eigenvalue $y_1 = -93.743$. The positive eigenvalues are the weak eigenvalue $y_2 = 0$ and the strong eigenvalue $y_3 = 85.004454910662$ with eigenvectors

$$\mathbf{v}_2 = \begin{pmatrix} 0 \\ 0 \\ 1 \end{pmatrix} \qquad \text{and} \qquad \mathbf{v}_3 = \begin{pmatrix} 8.140\,3 \times 10^{-5} \\ -1 \\ -1.990\,1 \times 10^{-5} \end{pmatrix} \tag{C.4}$$

respectively. Since the eigenvalue $y_2 = 0$ (corresponding to a vertical eigenvector), we need to evaluate $dS_w/d\xi$ slightly above and below the equilibrium point.

In Section D, we see that $dS_w/d\xi$ is positive above and below the equilibrium point. It is necessary to understand the behavior of the field on the plane generated by $\mathbf{v}_2$ and $\mathbf{v}_3$, near the equilibrium point.

Therefore the unstable manifold $W^u(-)$ (along which the orbits depart from $(-)$) is two-dimensional. It contains the point $(-)$ and it is tangent at that point to the vectors $\mathbf{v}_2$ and $\mathbf{v}_3$.

It is not hard to verify $dQ/d\xi = 0$ and $dT/d\xi = 0$ is zero along the line $T = T^b$ and $Q = 0$. Thus this line consists of orbits for the full system. Because it corresponds to the weakest eigenvalue all orbits tangent to this plane are also tangent to this line at the equilibrium point. The conjectured picture is again summarized in Figure F.1. Note that we have not drawn the Figure to scale in order to enhance its illustrative purpose.

Appendix D. Blow up of the upstream equilibrium for the steam condensation wave

When an injection saturation above the saturation $S_\dagger = 0.30804203989471$ is used ($S_\dagger$ is obtained from the equality of the saturation wave velocity and the steam condensation front velocity) we have two possible upstream equilibrium points, with $T = T^b$ and $Q = 0$. There are two "left" equilibrium points: (the first one is for $S_w = 0.30804203989471$, and the second one is for $S_w = 0.99143502200070$, corresponding to the definitions of $S_{\dagger\dagger}$ and $S_\dagger$ respectively). It turns out that the second equilibrium point is not admissible. As to the first equilibrium point, since its eigenvalue y_2 vanishes (corresponding to a vertical eigenvector), we need to evaluate $dS_w/d\xi$ slightly above and below the equilibrium point to facilitate the determination of the phase portrait near the nonhyperbolic equilibrium. As an example we use the situation that the lower saturation point $S_{w1} = 0.28569153532995$ and the higher saturation equilibrium point is 0.32804203989471, i.e. 0.02 above the usual equilibrium point. The steam condensation front velocity changes from $7.3840124530689 \times 10^{-6}$ [m/s] for $S_w = S_\dagger$ to $7.4068108367982 \times 10^{-6}$ [m/s] for both other cases.

D.1. **Local analysis of the lower saturation state at the upstream side.** We consider the upstream state with $Q = 0$, $T = T^b = 373.15$ and $S_{w1} = 0.28569153532995$.

Thus the left equilibrium $(-)$ for the ODE is

$$\left(Q^-, T^-, S_w^-\right) = (0, 293, 0.28569153532995)\,.$$

The Jacobian at the minus side is as follows:

$$J = \begin{pmatrix} 0 & -6.7195796010544 \times 10^{-3} & 0 \\ -1.1516024651448 \times 10^{6} & -8.7392206457278 & 0 \\ -22.425439884721 & 5.5791352471084 \times 10^{-5} & 0.025143208192761 \end{pmatrix}. \tag{D.1}$$

There is one eigenvalue $y_1 = -92.446$. The positive eigenvalues are the weak eigenvalue $y_2 = 0.025143208192761$ and the strong eigenvalue $y_3 = 83.706367830572$ with eigenvectors

$$\mathbf{v}_2 = \begin{pmatrix} 0 \\ 0 \\ 1 \end{pmatrix} \qquad \text{and} \qquad \mathbf{v}_3 = \begin{pmatrix} 2.2179 \times 10^{-5} \\ 1 \\ -8.0276 \times 10^{-5} \end{pmatrix}. \tag{D.2}$$

We get that $dS_w/d\xi$ is positive above and below the equilibrium point.

Therefore the unstable manifold $W^u(-)$ (along which the orbits depart from $(-)$) is two dimensional. It contains the point $(-)$ and it is tangent at that point to the vectors $\mathbf{v}_2$ and $\mathbf{v}_3$. Note, however, that the velocity of the saturation rarefaction wave exceeds the steam condensation front velocity, therefore this situation is not considered in the computations.

It is not hard to verify $dQ/d\xi = 0$ and $dT/d\xi = 0$ is zero along the line $T = T^b$ and $Q = 0$. Thus this line consists of orbits for the full system. Because it corresponds to the weakest eigenvalue all orbits tangent to this plane are also tangent to this line at the equilibrium point. The conjectured picture is again summarized in Figure F.1. Note that we have not drawn the figure to scale to enhance its illustrative purpose

D.2. **Local analysis of the higher saturation state.** We consider the upstream state with $Q = 0$, $T = T^b = 373.15$ and $S_{w2} = 0.32804203989471$.

Thus the left equilibrium $(-)$ for the ODE is

$$\left(Q^-, T^-, S_w^-\right) = (0, 293, 0.32804203989471)\,. \tag{D.3}$$

The Jacobian at the minus side is as follows:

$$J = \begin{pmatrix} 0 & -6.9195796010545 \times 10^{-3} & 0 \\ -1.1516024651448 \times 10^{6} & -8.7389251829442 & 0 \\ -20.330947447114 & 3.6720211572508 \times 10^{-5} & 0 \end{pmatrix}. \tag{D.4}$$

There is one negative eigenvalue $y_1 = -92.446$ The positive eigenvalues are the weak eigenvalue $y_2 = 0.025143208192761$ and the strong eigenvalue $y_3 = 85.004454910662$ with eigenvectors

$$\mathbf{v}_2 = \begin{pmatrix} 0 \\ 0 \\ 1 \end{pmatrix} \qquad \text{and} \qquad \mathbf{v}_3 = \begin{pmatrix} 2.2179 \times 10^{-5} \\ 1.0 \\ -8.0276 \times 10^{-5} \end{pmatrix}. \tag{D.5}$$

We get that $dS_w/d\xi$ is positive above and negative below the equilibrium point. It is necessary to understand the behavior of the field on the plane generated by $\mathbf{v}_2$ and $\mathbf{v}_3$, near the equilibrium point.

Therefore the unstable manifold $W^u(-)$ (along which the orbits depart from $(-)$) is two dimensional. It contains the point $(-)$ and it is tangent at that point to the vectors $\mathbf{v}_2$ and $\mathbf{v}_3$.

It is not hard to verify $dQ/d\xi = 0$ and $dT/d\xi = 0$ is zero along the line $T = T^b$ and $Q = 0$. Thus this line is an orbit for the full system. Because it corresponds to the weakest eigenvalue all orbits tangent to this plane are also tangent to this line at the equilibrium point. The conjectured picture is again summarized in Figure F.1. Note that we have not drawn the figure to scale to enhance its illustrative purpose.

Appendix E. Backward blow up of the steam condensation front

In this section, we assume that time and distance have been scaled so that the diffusion terms and the heat condensation terms balance, so that the Steam Condensation Zone has width $O(1)$; it will be studied as a travelling wave extending from $-\infty$ to $+\infty$. In the steam condensation zone capillary pressure effects, conduction, as well as mass and heat transfer terms have all to be taken into account. However, because this zone is thin relative to the zone spanned by the whole, we are always justified in ignoring pressure variation effects on densities within the zone.

For the analysis of travelling waves, it is advantageous to define the cumulative condensation distribution $Q(x,t)$ and cumulative condensation $Q^+(t)$ by

$$Q(x,t) = \int_{-\infty}^{x} q(x',t)dx', \qquad Q^+(t) = \int_{-\infty}^{+\infty} q(x',t)dx'. \tag{E.1}$$

Let us assume that all quantities depend only on $\xi = x - v^{SCF}t$. Now equations (1.14) – (1.16) and (E.1) can be written as

$$-\varphi v^{SCF} \frac{d(\rho_w S_w)}{d\xi} + \frac{d(\rho_w u f_w)}{d\xi} = \frac{dQ}{d\xi} + \frac{d}{d\xi}\left(\rho_w \Omega \frac{dS_w}{d\xi}\right), \tag{E.2}$$

$$-\varphi v^{SCF} \frac{d(\rho_g S_g)}{d\xi} + \frac{d(\rho_g u f_g)}{d\xi} = -\frac{dQ}{d\xi} - \frac{d}{d\xi}\left(\rho_g \Omega \frac{dS_w}{d\xi}\right), \tag{E.3}$$

$$\begin{aligned} -v^{SCF}\frac{d}{d\xi}\left(H_r + \varphi H_w S_w + \varphi H_g^s S_g\right) + \frac{d}{d\xi}\left(u\left(H_w f_w + H_g^s f_g\right)\right) = \\ = \Lambda \frac{dQ}{d\xi} + \frac{d}{d\xi}\left(\left(H_w - H_g^s\right)\Omega \frac{dS_w}{d\xi}\right) + \frac{d}{d\xi}\left(\kappa \frac{dT}{d\xi}\right), \end{aligned} \tag{E.4}$$

$$\frac{dQ}{d\xi} = q. \tag{E.5}$$

We integrate Eqs. (E.2) – (E.4) from ξ to ∞ once and use that $\frac{dS_w}{d\xi} \to 0$, $Q \to Q^+$ and $\frac{dT}{d\xi} \to 0$ for $\xi \to +\infty$, in such a way that $S_w \to S_w^+$ and $T \to T^+$, obtaining

$$-\rho_w \Omega \frac{dS_w}{d\xi} = (-Q^+ - \varphi v^{SCF} \rho_w^+ S_w^+ + \rho_w^+ u^+ f_w^+) - (-Q - \varphi v^{SCF} \rho_w S_w + \rho_w u f_w), \tag{E.6}$$

$$-\rho_g \Omega \frac{dS_w}{d\xi} = (-Q^+ + \varphi v^{SCF} \rho_g^+ S_g^+ - \rho_g^+ u^+ f_g^+) - (-Q + \varphi v^{SCF} \rho_g S_g - \rho_g u f_g), \tag{E.7}$$

$$\begin{aligned} -(H_w - H_g^s)\Omega \frac{dS_w}{d\xi} - \kappa \frac{dT}{d\xi} &= u^+(H_w^+ f_w^+ + H_g^{s+} f_g^+) - v^{SCF}(H_r^+ + \varphi H_w^+ S_w^+ + \varphi H_g^{s+} S_g^+) \\ &\quad - u(H_w f_w + H_g^s f_g) + v^{SCF}(H_r + \varphi H_w S_w + \varphi H_g^s S_g) - \Lambda(Q^+ - Q), \end{aligned} \tag{E.8}$$

$$\frac{dQ}{d\xi} = q. \tag{E.9}$$

Remark 18. *By letting ξ tend to $-\infty$ in Eq.* (E.6)*, we recover the Rankine–Hugoniot condition:*

$$Q^+ = u^+ \rho_w^+ f_w^+ - u^- \rho_w^- f_w^- - \varphi v^{SCF} (\rho_w^+ S_w^+ - \rho_w^- S_w^-), \tag{E.10}$$

and since $S_g^+ = 0$, it follows from Eq. (E.7) *that*

$$Q^+ = \rho_g^- \left(u^- f_g^- - \varphi v^{SCF} S_g^- \right). \tag{E.11}$$

A similar limiting procedure in Eq. (E.8) *recovers the other Rankine–Hugoniot condition:*

$$\begin{aligned} \Lambda Q^+ &= u^+(H_w^+ f_w^+ + H_g^{s+} f_g^+) - u^-(H_w^- f_w^- + H_g^{s-} f_g^-) \\ -v^{SCF}&\Big[(H_r^+ + \varphi H_w^+ S_w^+ + \varphi H_g^{s+} S_g^+) - (H_r^- + \varphi H_w^- S_w^- + \varphi H_g^{s-} S_g^-)\Big]. \end{aligned} \tag{E.12}$$

We can divide the equations (E.6), (E.7) by the densities, and take advantage of the fact that $S_g^+ = f_g^+ = 0$, $S_w^+ = f_w^+ = 1$, obtaining

$$-\Omega \frac{dS_w}{d\xi} = -\left(-\frac{Q}{\rho_w} - \varphi v^{SCF} S_w + u f_w \right) + \left(-\frac{Q^+}{\rho_w} + \frac{\rho_w^+}{\rho_w}\Big(-\varphi v^{SCF} + u^+ \Big) \right), \tag{E.13}$$

$$-\Omega \frac{dS_w}{d\xi} = -\left(-\frac{Q}{\rho_g} + \varphi v^{SCF} S_g - u f_g \right) + \left(-\frac{Q^+}{\rho_g} \right). \tag{E.14}$$

Subtracting Eq. (E.14) from Eq. (E.13) we obtain $u = u(Q, T)$ as

$$u = -(Q^+ - Q)\left(\frac{1}{\rho_w} - \frac{1}{\rho_g} \right) + \varphi v^{SCF} + \frac{\rho_w^+}{\rho_w}\left(-\varphi v^{SCF} + u^+ \right). \tag{E.15}$$

Remark 19. *Letting $\xi \to -\infty$ in Eq.* (E.15)*, we obtain*

$$u^+ = -Q^+ \left(\frac{1}{\rho_w^-} - \frac{1}{\rho_g^-} \right) + \varphi v^{SCF} + \frac{\rho_w^+}{\rho_w^-}\left(u^+ - \varphi v^{SCF} \right). \tag{E.16}$$

Of course, this equation can also be obtained from Eqs. (E.10) *and* (E.11)

Multiplying Eq. (E.13) by H_w, Eq. (E.14) by H_g^s and subtracting we obtain

$$\begin{aligned} &-\left(H_w - H_g^s\right)\Omega\frac{dS_w}{d\xi} = -(Q^+ - Q)\left(\frac{H_w}{\rho_w} - \frac{H_g^s}{\rho_g}\right) + \varphi v^{SCF}\left(H_w S_w + H_g^s S_g\right) \\ &-u\left(H_w f_w + H_g^s f_g\right) + \frac{\rho_w^+}{\rho_w} H_w\left(-\varphi v^{SCF} + u^+\right). \end{aligned} \tag{E.17}$$

Subtracting this equation from Eq. (E.8), and taking advantage of the fact that $S_g^+ = f_g^+ = 0$, $S_w^+ = f_w^+ = 1$, we obtain

$$-\kappa\frac{\partial T}{\partial \xi} = (Q^+ - Q)\left(\frac{H_w}{\rho_w} - \frac{H_g^s}{\rho_g} - \Lambda\right) - u^+\rho_w^+\left(\frac{H_w^+}{\rho_w^+} - \frac{H_w}{\rho_w}\right)$$

$$-v^{SCF}(H_r^+ - H_r) - \varphi v^{SCF}\rho_w^+\left(\frac{H_w^+}{\rho_w^+} - \frac{H_w}{\rho_w}\right). \tag{E.18}$$

The enthalpies used above are only functions of temperature. Note that the ratios of the enthalpies per unit volume and the densities can be interpreted as enthalpies per unit mass. Thus, it is useful to define enthalpies per unit mass $h_w(T)$, $h_r(T)$, $h_g(T)$ ($[J/kg]$) as enthalpies per unit volume H_r, H_w, H_g ($[J/m^3]$) divided by the respective densities at the temperature of interest.

Subtracting Eq. (E.6) from Eq. (E.7) we obtain

$$\begin{aligned} (\rho_w - \rho_g)\Omega\frac{dS_w}{d\xi} =& -\varphi v^{SCF}(\rho_w S_w + \rho_g S_g) - u(\rho_w f_w + \rho_g f_g) \\ &+ \varphi v^{SCF}\rho_w^+ S_w^+ + u^+\rho_w^+ f_w^+. \end{aligned} \tag{E.19}$$

If we divide the RHS of Eq. (E.19) by ρ_w, and choose v^{SCF} as given by Eq. (2.33), we see that (S_w, S_g, u) given by (S_w^-, S_g^-, u^-) and $(S_w^+ = 1, S_g^+ = 0, u^+)$ where u^+ is given by Eq. (2.32), $S_w^+ < S_w^*$, $S_g^+ = 1 - S_w^+$ are equilibria for the ordinary differential equation (E.19).

For an orbit to exist between the equilibria $(-)$ and $(+)$, it is necessary and sufficient that there is no other equilibrium in between, yielding Oleĭnik's construction.

To plot conveniently, the independent variables will be reordered as Q, T, S_w. We obtain the following ODE's to be analyzed, with fluxes given by F^Q, $\kappa^{-1}F^T$, and $\Omega^{-1}F^w$ defined below. From Eqs. (A.9) and (1.13):

$$\frac{dQ}{d\xi} = q_b\left(S_w - 1\right)\left(T - T^b\right) := F^Q \tag{E.20}$$

From Eq. (E.18), we divide by κ:

$$\frac{\partial T}{\partial \xi} = \kappa^{-1}\Bigg((Q^+ - Q)\left(\frac{H_w}{\rho_w} - \frac{H_g^s}{\rho_g} - \Lambda\right) - u^+\rho_w^+\left(\frac{H_w^+}{\rho_w^+} - \frac{H_w}{\rho_w}\right)$$
$$- v^{SCF}(H_r^+ - H_r) - \varphi v^{SCF}\rho_w^+\left(\frac{H_w^+}{\rho_w^+} - \frac{H_w}{\rho_w}\right)\Bigg) := \kappa^{-1}F^T. \tag{E.21}$$

From Eq. (E.19), dividing by $(\rho_w - \rho_g)\,\Omega$:

$$\frac{dS_w}{d\xi} = \Omega^{-1} - \left(\varphi v^{SCF}\left[S_w + \frac{\rho_g}{\rho_w - \rho_g} - \frac{\rho_w^+}{\rho_w - \rho_g}S_w^+\right] - u\left[f_w + \frac{\rho_g}{\rho_w - \rho_g}\right] + u^+f_w^+\rho_w^+\right) := \Omega^{-1}F^w. \tag{E.22}$$

Let us assume constant water and heat capacity, and constant water density. Eqs. (E.21), (E.22), (E.15) become:

$$\frac{\partial T}{\partial \xi} = \kappa^{-1}\Bigg((Q^+ - Q)\left(\Big(\frac{C_w}{\rho_w} - \frac{H_g^s}{\rho_g}\Big)(T - T^0) - \Lambda\right) - u^+C_w(T^+ - T)$$
$$- v^{SCF}C_w(T^+ - T) - \varphi v^{SCF}C_w(T^+ - T)\Bigg) := \kappa^{-1}F^T, \tag{E.23}$$

$$\frac{dS_w}{d\xi} = \Omega^{-1}\left(-\varphi v^{SCF}\left[S_w + \frac{\rho_g}{\rho_w - \rho_g} - \frac{\rho_w}{\rho_w - \rho_g}S_w^+\right] - u\left[f_w + \frac{\rho_g}{\rho_w - \rho_g}\right] + u^+f_w^+\rho_w\right) := \Omega^{-1}F^w, \tag{E.24}$$

$$u = -(Q^+ - Q)\left(\frac{1}{\rho_w} - \frac{1}{\rho_g}\right) + u^+. \tag{E.25}$$

Notice that the right hand side of Eq. (E.22) depends on the S_w, T and Q, while the right hand side of Eq. (E.21) depends on the T and Q, and the right hand side of Eq. (B.1) depends on the S_w and T.

Notice that approximating ρ_g/ρ_w by 0 in Eqs. (E.24), (E.25) causes an error $O(\rho_g/\partial\rho_w)$, which is typically very small. If we make this approximation, the right hand side of Eq. (E.24) depends only on S_w and Q.

Appendix F. The phase portrait

Lemma F.1. *On the edge $S_w = 1$ and $Q = Q^+$ the quantity F^w vanishes for all T.*

A tedious but straightforward calculation shows that $F^w = 0$, starting from equations A.7, A.15 and B.3 on the edge $S_w = 1$ and $Q = Q^+$.

From Lemma F.1 and the calculations in Appendix C, Section C.1, it follows that the stable manifold of the downstream state (+) locally has the attractor saddle structure shown in Fig. F.1.

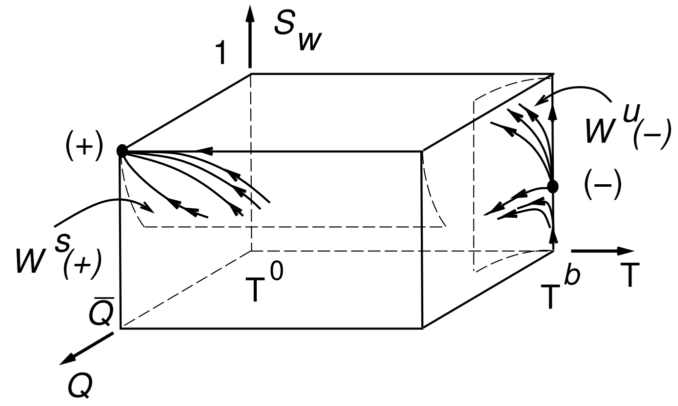

FIGURE F.1. SCF structure in phase state near $(-)$ and $(+)$ equilibria.

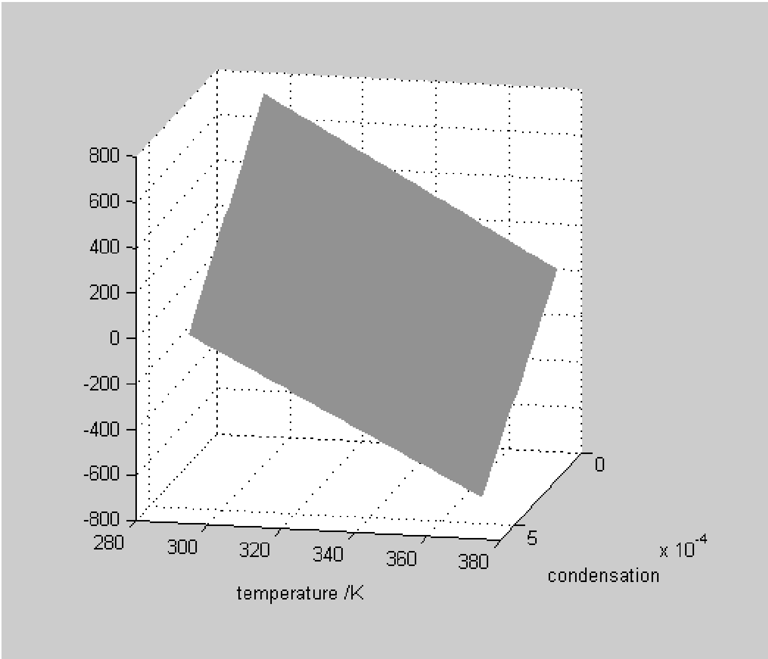

FIGURE F.2. $\kappa^{-1}F^T$ as a function of T and Q, Eq. (B.2).

By collapsing the two perturbed upstream $(-)$ states analyzed in Appendix D, it follows that the unstable manifold at the state $(-)$ locally has the repeller saddle-node structure shown in Fig. F.2.

We conjecture that the two manifolds intersect transversally; this intersection is a unique orbit between the $(-)$ and $(+)$ state. To support this conjecture, we show in Fig. F.2 the temperature component $\kappa^{-1}F^T$ of the vector field as a function of the temperature T and the cumulative condensation Q. We see that this component in always positive in the range of the temperature of interest. Thus the temperature should be monotone decreasing along the SCF profile.

The surfaces where the field is horizontal are represented in Fig. F.3.

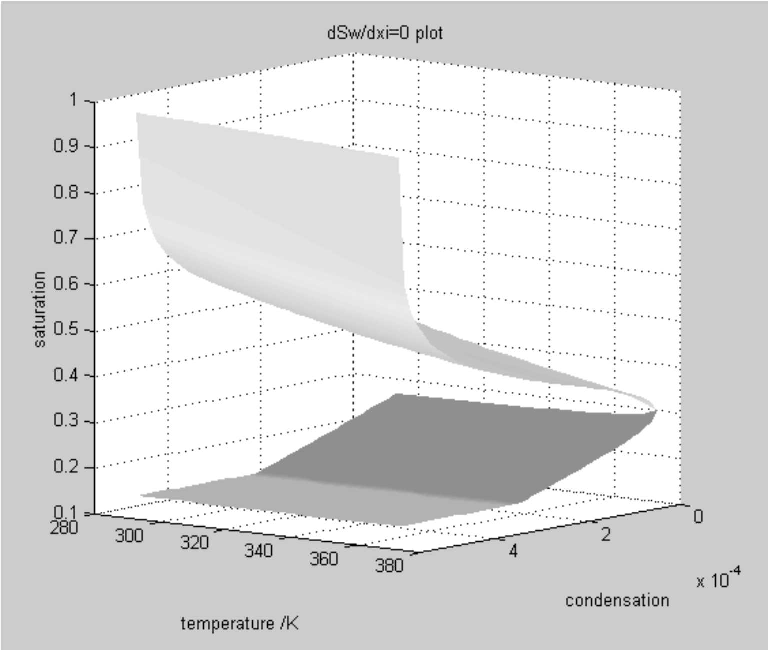

FIGURE F.3. Locus where $\mathcal{F}^w$ vanishes, Eq. (B.3).

The vertical component $\Omega^{-1}\mathcal{F}^w$ is negative within the two surfaces and positive outside. The two branches of the surface touch precisely at the $(-)$ equilibrium. The orbit we are seeking must exit the $(-)$ equilibrium upwards vertically; that is, they are all tangent to the orbit contained in the edge $T = T^b$; $Q = Q^b$. We conjecture that it stays above the top surface branch, so that the saturation is monotone increasing along the SCF profile.

The top surface gets out of the front $Q = Q^+$ and folds back returning to the edge $Q = Q^+$ and $S_w = 1$.

These surfaces were obtained numerically. It is easy to see that the surfaces in Fig. F.3 have the form $F_w(s, Q, T) = 0$ with very weak dependence on T. This is so because the temperature dependence of F_w (in Eq. (B.3)) is due to ρ_w, which is almost constant in T, and to ρ_g, which is very small compared to other densities.

APPENDIX G. PHYSICAL QUANTITIES; SYMBOLS AND VALUES

In this Appendix we summarize the values and units of the various quantities used in the computation and empirical expressions for the various parameter functions. For convenience we express the heat capacity of the rock C_r^p in terms of energy per unit volume of *porous medium* per unit temperature *i.e.* the factor $1 - \varphi$ is already included in the rock density. All other densities are expressed in terms of mass per unit volume of the phase.

Table 2, Summary of physical input parameters and variables

Physical quantity	*Symbol*	*Value*	*Unit*
Temperature derivatives of enthalpies	c_w^p, c_g^p	$dh_w/dT, dh_g/dT$	[J/(kgK)]
Water, steam fractional functions	f_w, f_g	Eq. (1.11).	[m^3/m^3]
Water-steam frac. flow, hot region	f_w^b, f_g^b		[m^3/(m^{2}s)]
Porous rock permeability	k	1.0×10^{-12}	[m^3]
Water, steam relative permeabilities	k_{rw}, k_{rg}	Eq. (G.10), (G.11).	[m^3/m^3]
Pressure	p	1.0135×10^5	[Pa]
Mass condensation rate	q	Eq. (1.3).	[kg /(m^{3}s)]
Mass condensation rate coefficient	q^b	0.01	[kg /(m^{3}sK)]
Steam injection rate	u^{inj}	9.52×10^{-4}	[m^3/(m^{2}s)]
Water, steam phase velocity	u_w, u_g	Eq. (1.2).	[m^3/(m^{2}s)]
Total Darcy velocity	u	$u_w + u_g$, Eq. (1.13).	[m^3/(m^{2}s)]
Flow rate in hot region	u^b	Eq. (2.6).	[m^3/(m^{2}s)]
Flow rate in cold water zone	u^0	Eq. (2.22).	[m^3/(m^{2}s)]
Flow rate in hot water zone	u^b	Eq. (2.25).	[m^3/(m^{2}s)]
SCF velocity	v^{SCF}	Eq. (2.33).	[m/s]
Cooling contact disc. speed, hot water zone	v_w^b	Eq. (2.27).	[m/s]
Thermal characteristic speed, cold water zone	v^0	Eq. (2.37).	[m/s]
Water thermal characteristic speed	v_w	Eq. (2.15).	[m/s]
Water thermal shock speed	$v_w^{T,0}$	Eqs. (2.19) / (2.21).	[m/s]
Saturation characteristic speed, hot region	v_s^b	Eq. (2.7).	[m/s]
Hot isothermal steam-water shock velocity	$v_{g,w}^b$	Eq. (2.8).	[m/s]
Cooling contact discontinuity velocity	$v_w^{b,0}$	Eq. (2.26).	[m/s]
Water, steam heat capacity *	C_w^p, C_g^p	$dH_w/dT, dH_g^s/dT$	[J/(m^{3}K)]
Effective rock heat capacity	C_r^p	2.029×10^6	[J/(m^{3}K)]
Steam enthalpy	H_g	$\rho_g(T)\big(h_g(T) - h_w(T^0)\big)$	[J/m^3]
Steam sensible heat	H_g^s	Eq. (G.5).	[J/m^3]
Steam latent heat	H_g^l	$\rho_g(T)\Lambda^0$	[J/m^3]
Rock enthalpy	H_r	$\rho_r C_r^p(T - T^0)$	[J/m^3]
Water enthalpy	H_w	$\rho_w(T)\big(h_w(T) - h_w(T^0)\big)$	[J/m^3]
Water, rock enthalpy at boiling temperature	H_w^b, H_r^b	$H_w(T^b)$, $H_r(T^b)$	[J/m^3]
Steam total and sensible enthalpy at boil. temp.	H_g^B, H_g^b	Eq. (2.34).	[J/m^3]
Water, rock enthalpy, reservoir temperature	H_w^0, H_r^0	$H_w(T^0)$, $H_r(T^0)$	[J/m^3]
Capillary pressure	P_c	Eq. (G.12).	[Pa]
Cumulative mass condensation	Q	Eq. (A.1).	[kg /m^3]
Water, steam saturations	S_w, S_g	Dependent variables.	[m^3/m^3]
Connate water saturation	S_{wc}	0.15	[m^3/m^3]
Water injection saturation	S_w^{inj}	See Section 4.	[m^3/m^3]
Water effective saturation	S_{we}	$(S_w - S_{wc})/(1 - S_{wc})$	[-]
Steam effective saturation	S_{ge}	$S_g/(1 - S_{wc})$	[-]
Hot-cold bifurcation water saturation	S_*	Theorem 1.	[m^3/m^3]
Steam-water bifurcation water saturation	$S_\dagger$	Eq. (3.7).	[m^3/m^3]
Second bifurcation ghost saturation	$S_{\dagger\dagger}$	See Remark 11.	[m^3/m^3]
Water saturation at inflection	S^{infl}	Frac. flow infl. sat.	[m^3/m^3]

Table 3, Summary of physical input parameters and variables

Physical quantity	*Symbol*	*Value*	*Unit*
Temperature	T	Dependent variable.	[K]
Reservoir temperature	T^0	293.	[K]
Boiling point of water–steam	T^b	Eq. (G.1).	[K]
Steam thermal expansion coefficient *	α_g	$-(1/\rho_g)(\partial\rho_g/\partial T)_p$	[/K]
Water thermal expansion coefficient	α_w	$-(1/\rho_w)(\partial\rho_w/\partial T)_p$	[/K]
Water, steam thermal conductivity	κ_w, κ_g	0.652, 0.0208	[W/(mK)]
Rock, composite thermal conductivity	κ_r, κ	1.83, Eq. (1.7).	[W/(mK)]
Saturation exponent for P_c	λ_s	0.5, Eq. (G.12)	[-]
Water, steam viscosity	μ_w, μ_g	Eq. (G.7), Eq. (G.6).	[Pa s]
Water, steam densities	ρ_w, ρ_g	Eq. (G.9), Eq. (G.8).	[kg/m^3]
Water, steam, rock densities - boiling temp.	ρ_w^b, ρ_g^b, ρ_r^b	Eq. (2.23)	[kg/m^3]
Water, steam, rock densities - reservoir temp.	ρ_w^0, ρ_g^0, ρ_r^0		[kg/m^3]
Interfacial tension	σ_{wg}	58×10^{-3}	[N/m]
Rock porosity	φ	0.38	[m^3/m^3]
Water evaporation heat	Λ^0	Eq. (1.1).	[J/kg]
Capillary diffusion coefficient	Ω	Eqs. (1.10), (1.12).	[m^3/m^3]

G.1. **Temperature dependent properties of steam and water.** We use reference [29] to obtain all the temperature dependent properties below. The water and steam densities used to obtain the enthalpies are defined at the bottom. First we obtain the boiling point T^b at the given pressure p, *i.e.*

$$T^b = 280.034 + \ell(14.0856 + \ell(1.38075 + \ell(-0.101806 + 0.019017\ell))), \tag{G.1}$$

where $\ell = \log(p)$ and p is the pressure in [k Pa]. The evaporation heat [J/kg] is given as a function of the temperature T at which the evaporation occurs. We use atmospheric pressure ($p = 101.325$ [k Pa]) in our computations, to make the example is representative of subsurface contaminant cleaning.

The liquid water enthalpy $h_w(T)$ [J/kg] as a function of temperature is approximated by

$$h_w(T) = 2.36652 \times 10^7 - 3.66232 \times 10^5 T + 2.26952 \times 10^3 T^2 - 7.30365 T^3 + 1.30241 \times 10^{-2} T^4$$
$$-1.22103 \times 10^{-5} T^5 + 4.70878 \times 10^{-9} T^6. \tag{G.2}$$

The steam enthalpy h_g [J/kg] as a function of temperature is approximated by

$$\begin{aligned} h_g = &-2.20269 \times 10^7 + 3.65317 \times 10^5 T - 2.25837 \times 10^3 T^2 + 7.3742 T^3 \\ &-1.33437 \times 10^{-2} T^4 + 1.26913 \times 10^{-5} T^5 - 4.9688 \times 10^{-9} T^6. \end{aligned} \tag{G.3}$$

For the latent heat h_g^l [J/kg] or evaporation heat $\Lambda(T)$ we obtain

$$h_g^l = \left(7.1845 \times 10^{12} + 1.10486 \times 10^{10} T - 8.8405 \times 10^7 T^2 + 1.6256 \times 10^5 T^3 - 121.377 T^4\right)^{\frac{1}{2}}. \tag{G.4}$$

The sensible heat of steam $H_g^s(T)$ in [J/m^3] is given as

$$H_g^s(T) = \rho_g \left(h_g(T) - h_w\left(T^0\right) - \Lambda\left(T^0\right)\right). \tag{G.5}$$

We also use the temperature dependent steam viscosity

$$\mu_g = -5.46807 \times 10^{-4} + 6.89490 \times 10^{-6} T - 3.39999 \times 10^{-8} T^2 + 8.29842 \times 10^{-11} T^3$$
$$-9.97060 \times 10^{-14} T^4 + 4.71914 \times 10^{-17} T^5. \tag{G.6}$$

The temperature dependent water viscosity μ_w is approximated by

$$\mu_w = -0.0123274 + \frac{27.1038}{T} - \frac{23527.5}{T^2} + \frac{1.01425 \times 10^7}{T^3} - \frac{2.17342 \times 10^9}{T^4} + \frac{1.86935 \times 10^{11}}{T^5}. \tag{G.7}$$

For the steam density as a function of temperature $T[K]$ we use a different expression than [29] because our interest is a steam density at constant pressure, which is not necessarily in equilibrium with liquid water.

$$\rho_g(T) = p \frac{M_{H_2O}}{ZRT} \tag{G.8}$$

where p is the pressure, R=8.31 [J/mol K] and Z is the Z-factor (see e.g. Dake [7]). For the atmospheric pressures of interest here the Z-factor is close to unity. The liquid water density as a function of the temperature $T[K]$ is given as

$$\rho_w(T) = 3786.31 - 37.2487T + 0.196246T^2 - 5.04708 \times 10^{-4} T^3$$
$$+6.29368 \times 10^{-7} T^4 - 3.08480 \times 10^{-10} T^5. \tag{G.9}$$

G.2. **Constitutive relations.** The relative permeability functions k_{rw} and k_{rg} are considered to be power functions of their respective saturations [9], *i.e.*

$$k_{rw} = \begin{cases} \left(\frac{S_w - S_{wc}}{1 - S_{wc}}\right)^{n_w} & \text{for} \quad S_w \geq S_{wc}, \\ 0 & \text{for} \quad 0 \leq S_w \leq S_{wc}, \end{cases} \tag{G.10}$$

$$k_{rg} = \left(\frac{S_g}{1 - S_{wc}}\right)^{n_g}. \tag{G.11}$$

For the computations we take $n_w = 4, = n_g = 2$. The connate water saturation S_{wc} is given in the table.

The capillary pressure is of the Brooks-Corey type and we use the dimensionless capillary pressure $P_c(S_w = 0.5)/\left(\sigma_{wg}\sqrt{\varphi/k}\right) = 0.5$ which is appropriate for many sandstones. The capillary pressure between steam and water is given by the empirical expression which combines Leverett's approach to non-dimensionalize the capillary pressure [14] with the semi-empirically determined saturation dependence suggested by Brooks [5]:

$$P_c = \sigma_{wg}\gamma\sqrt{\frac{\varphi}{k}} \left(\frac{\frac{1}{2} - S_{wc}}{1 - S_{wc}}\right)^{\frac{1}{\lambda_s}} \left(\frac{S_w - S_{wc}}{1 - S_{wc}}\right)^{-\frac{1}{\lambda_s}}, \tag{G.12}$$

where γ is a parameter that in many cases assumes values between 0.3 and 0.7. We use $\gamma = 0.5$ and $\lambda_s = \frac{1}{2}$. Finally $\sigma_{wg} = 0.058$ N/m is the water-vapor interfacial tension. We disregard its temperature dependence and use the value at the boiling point (see [31], p. F-45). We present the equation in its present form to stress its dependence on the effective saturation $S_{we} = (S_w - S_{wc})/(1 - S_{wc})$.

References

[1] AYDELOTTE, S.R., and POPE, G.A., *A Simplified Predictive Model for Steamdrive Performance*, J. Pet. Techn. (May 1983), 991-1002.

[2] BEAR, J., *Dynamics of Fluids in Porous Media* , p. 650 and 651, Dover Publications, Inc., New York (1972).

[3] BEEK, W.J., and MUTTZALL, M.K., *Transport Phenomena*, John Wiley & Sons (1975), page 198.

[4] BIRD, R.B., STEWART, W.E., and LIGHTFOOT, E.N., *Transport Phenomena*, John Wiley & Sons (1960).

[5] BROOKS, R.H., and COREY, A.T., *Properties of porous media affecting fluid flow*, J. Irr. Drain. Div., Proc., Am. Soc. Civ. Eng. June (1966), 61-88.

[6] BRUINING, J., and DUIJN, C.J., *Uniqueness Conditions in a Hyperbolic Model for Oil Recovery by Steamdrive*, Computational Geosciences **4**, 65-98 (2000).

[7] DAKE, L.P., *Fundamentals of Reservoir Engineering*, Elsevier Science Publishers, Amsterdam, 1978.

[8] VAN DUIJN, C.J., *Uniqueness conditions in a hyperbolic model for oil recovery by steamdrive*, Book of Abstracts - Seventh International International Conference on Hyperbolic Problems, Theory, Numerics, Applications - Zürich, 1998.

[9] DULLIEN, F.A.L., *Porous media; fluid transport and pore structure*, Academic Press, N.Y. (1979).

[10] DYKE, M. VAN., *Perturbation Methods in Fluid Mechanics*, Chapter 5, The Parabolic Press, Stanford, 1975.

[11] ISAACSON, E., MARCHESIN, D., PLOHR, B., and TEMPLE, J.B., *Multiphase flow models with singular Riemann problems*, Mat. Apl. Comput., **11**, n. 2, 147-166, 1992.

[12] HUNT, J.R., SITAR, N., and UDELL, K., Water Resour. Res. **24**, 1247 (1988).

[13] ISAACSON, E., MARCHESIN, D., and PLOHR, B., *Transitional waves for conservation laws*, SIAM J. Math. Anal., **21**, 837-866, 1990.

[14] LEVERETT, M.C., *Capillary behavior in porous solids*, Trans., AIME, **142**, 142-169, 1941.

[15] MANDL, G.W., and VOLEK, C.W., *Heat and mass transport in steamdrive processes*, SPEJ, 57-79, March 1969.

[16] MARX, J.W., and LANGENHEIM, R.H., *Reservoir heating by hot fluid injection*, Trans., AIME Vol **216**, 312 (1959).

[17] MENEGUS, D.K., and UDELL, K.S., *A study of steam injection into water saturated capillary porous media*, Heat Transfer in Porous Media and Particulate Flows, ASME Heat Transfer Div., New York City, **46**, 151-157, 1985.

[18] OLEĬNIK, O., *Discontinuous Solutions of Nonlinear Differential Equations*, Usp. Mat. Nauk. (N. S.) v.12, pp. 3-73, 1957. English transl. in Amer. Math Soc. Transl. Ser. 2, 26, 95-172.

[19] PERRY, R.H., and GREEN, D.W., Eds., *Perry's chemical engineers' handbook*, Sixth edition ISBN 0-07-049479-7, McGraw-Hill (1984), table 3-320.

[20] PETERSON, P.F., *Diffusion Layer Modeling for Condensation with Multicomponent Non-condensable Gases*, Journal of Heat Transfer, Transactions of the ASME, Vol **122**, 716-720 (2000).

[21] POPE, G.A., *The application of fractional flow theory to enhanced oil recovery*, SPEJ, 191-205, June 1980.

[22] PRATS, M., *Thermal Recovery*, Monograph Series, SPE, Richardson, TX (1982), **7**.

[23] SCHECTER, S., MARCHESIN, D., and PLOHR, B., *Classification of codimension-one Riemann solutions* , Journal of Dynamics and Differential Equations, vol. 13, no. 3, pp. 523-588, 2001.

[24] SHEARER, M., and TRANGENSTEIN, J.A., *Loss of real characteristics for models of three-phase flow in a porous medium*, Transp. Por. Med., **4**, 499-525, 1989.

[25] SHODA, A., WANG, C.Y., and CHENG, P., *Simulation of constant pressure steam injection in a porous medium*, Int. Comm. Heat Mass Transfer Vol **25** (6), 753-762 (1998).

[26] SHUTLER, N.D., *A one-dimensional analytical technique for predicting oil recovery by steamflooding*, SPEJ Dec (1972), 489-498.

[27] STEWART, L.D., and UDELL, K.S. *Mechanisms of residual oil displacement by steam injection*, SPE Reservoir Engineering, Nov (1988), 1233-1242.

[28] TAMIM, M., ABOU-KASSEM, J.H., and FAROUQ ALI, S.M., *Recent developments in numerical simulation techniques of thermal recovery processes*, Journal of Petroleum Engineering Science and Engineering **26**, 283-289 (2000).

[29] TORTIKE, W.S., and FAROUQ ALI, S.M., *Saturated-steam-property functional correlations for fully implicit reservoir simulation*, SPERE (November 1989) 471-474.

[30] UDELL, K.S., *Heat transfer in porous media considering phase change and capillarity- the heat pipe effect*, Intl. J. Heat Mass Transfer, **28**, 485-495 (1985).

[31] WEAST, R.C., *CRC Handbook of chemistry and physics*, 58^{th} edition, CRC Press, Inc. 1977-1978.

[32] WINGARD, J.S., and ORR, F.M., *An analytical solution for steam/oil/water displacements*, SPE Advanced Technology Series, Vol **2**, 2, 167-176 (1994).

[33] YORTSOS, Y.C., *Distribution of fluid phases within the steam zone in steam-injection processes*, SPEJ, 458-466, August 1984.

[34] YORTSOS, Y.C., and GAVALAS, G.R., *Heat transfer ahead of moving condensation fronts in thermal recovery processes*, Int. J. Heat and Mass Transfer, vol **25** (3) 305-316 (1982).

Appendix H. Properties of the injected substance and the Riemann solution

**** TO DO: USE NAME ORGANIZING CENTER FOR STATE ($*\dagger$) IN FIG. H.1.

We have seen in Sections 3 and 4 the importance of the hot-cold and steam-water bifurcation points. Here we address issues such as existence, and their impact on the structure of the Riemann solution.

Recall Fig. 3.3 showing the construction of the hot-cold bifurcation point $S_\dagger$. Assume that the physics of the substance in the reservoir that is also injected as a vapor at a higher temperature dictates the assumption

$$H_g^B - H_w^b > 0. \tag{H.1}$$

(Here we have maintained the subscripts w and g for the substance in the liquid and vapor form, respectively). Therefore, the conclusions in Eq. (3.10) follow. However, if $f^\dagger/S^\dagger$ is very large, $S_\dagger$ ceases to exist. In fact, we see that as soon as the straight line $(S^\dagger, f^\dagger)$, $(S_\dagger, f_\dagger^b)$ goes through the point $(S, f) = (1, 1)$, the shock from $S^\dagger$ to $S_\dagger$ ceases to be admissible (in the sense of Oleĭnik). It is convenient to define the point $(S_{*\dagger}, f_{*\dagger})$ as the tangency point of the line through $(1, 1)$ to the fractional flow curve. (See also Fig. 3.2).

Lemma H.1. *If $S_\dagger$ exists, then $0 \le S_\dagger < S_{*\dagger}$. If $f^\dagger/S^\dagger$ is larger than the slope $(1 - f_{*\dagger})/(1 - S_{*\dagger})$, then $S_\dagger$ does not exist. In this case there is no steam-water bifurcation, and there is no steam condensation front, as the left characteristics would be slower than this front. Therefore, the structure of the Riemann problem is always given by Case* III.

As to the hot-cold bifurcation, we see from the second equality in Eq. (3.1) that (S_*, f_*) is obtained graphically as S_* in Fig. 3.2. The point S_{**} solves the same equation, but the shock from S_{**} to 1 does not satisfy Oleĭnik's condition so it is not a genuine steam condensation front and it does not play any role in the Riemann solution. We see that $S_{*\dagger} < S_* < 1$. It is easy to see the following fact.

Lemma H.2. *If $H_w^b/(H_r^b + \varphi H_w^b)$ is too large, there is no S_*, no hot-cold bifurcation, and no steam condensation front. Thus, the structure of the Riemann solution is given by Cases* II *and* III. ****???****

Remark 20. *When $S_\dagger$ and S_* both exist, we have $S_\dagger \le S_*$.*

*** TO DO: MAKE VERSION OF Fig. H.1 WITH AXES S_w AND v ***

We summarize the situation in the schematic diagram in Fig. H.1.

This diagram shows how the relationship between thermal and hydrodynamical properties of the liquid and vapor phases affects the possible Riemann solutions structures, cases I, II, III.

It would be very interesting to generate a figure with independent variables T^0 and T^b, showing the surface $S_*(T^0, T^b)$, the surface $S_\dagger(T^0, T^b)$ and the curve where these two surfaces intersect. This intersection projected into the (T^0, T^b) plane is the curve of all possible $S_{*\dagger}$.

In this three-dimensional figure it would be possible to show all possible structures of Riemann solutions.

An intriguing possibility is to make the same figure in terms of independent variables T^0 and p (pressure). See Fig. H.2.

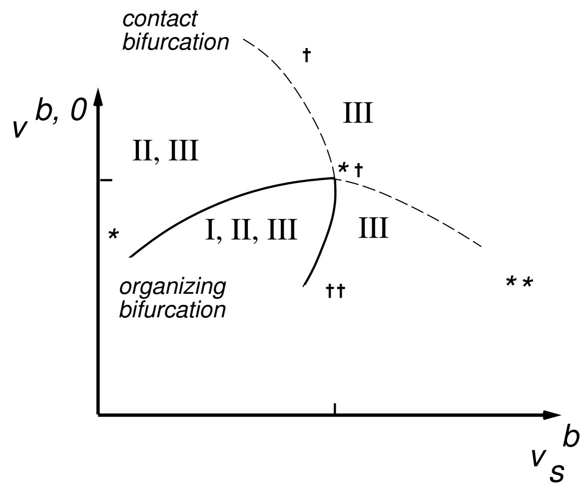

FIGURE H.1. Possible structures of Riemann solutions: bifurcation diagram in thermal/hydrodynamical parameter space. The axes are hot isothermal steam-water shock speed and the hot-cold shock speed. The $*\dagger$ point is extremum of speeds along each separation curve. At this point, $v^b_{g,w} = v^{b,0}_w = v^{SCF} = v^b_s$. ***IS THE FIGURE RIGHT? ** HB DOES NOT UNDERSTAND IT ***

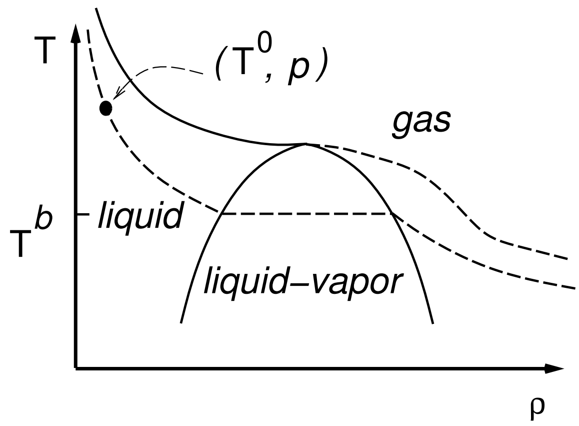

FIGURE H.2. Construction of mapping $(T^0, p) \to (T^0, T^b)$, using isobars. **** HB SAYS WE ARE ALWAYS IN THE LIQUID-VAPOR REGION; DAN SAYS THAT THE INITIAL CONDITIONS OF THE RESERVOIR ARE NOT NECESSARILY IN THE LIQUID-VAPOR REGION ***

Dietz Laboratory, Centre of Technical Geoscience, Mijnbouwstraat 120, 2628 RX Delft, The Netherlands
E-mail address: J.Bruining@mp.tudelft.nl

Instituto de Matemática Pura e Aplicada, Estrada Dona Castorina 110, 22460-320 Rio de Janeiro, RJ, Brazil
E-mail address: marchesi@impa.br

Technische Universiteit Eindhoven, Den Dolech 2, 5600 MB Eindhoven, The Netherlands
E-mail address: c.j.v.duijn@tue.nl